Rev. Adv. Mater. Sci. 53 (2018) 49-73

RECENT ADVANCES IN POROUS SILICON BASED OPTICAL BIOSENSORS

Nalin H. Maniya

Analytical Division & Centralized Instrument Facility, CSIR-Central Salt & Marine Chemicals Research Institute, Bhavnagar – 364 002, Gujarat, India

Received: July 04, 2017

Abstract. PSi structures have unique physical and optical properties, which are being exploited for a numerous biomedical applications including biosensing, bioimaging, tissue engineering, and drug delivery. Different PSi optical structures can be fabricated to improve the sensitivity of the optical measurements. A very high surface area per volume of PSi can be used for the higher loading of target analytes in a small sensor area, which helps in increasing sensitivity and allows the miniaturization of biosensor. The specificity of PSi biosensor to the target analyte can be inferred by immobilizing the corresponding bioreceptor such as DNA, enzyme, or antibody via different conjugation chemistries. Finally, PSi is biocompatible material that offers additional advantage in comparison to other sensing platforms for *in vivo* implantable biosensing applications. This paper reviews fabrication, surface modification, biofunctionalization, and optical biosensing applications of PSi structures with special emphasis on *in vivo* and PSi photonic particles biosensing.

1. INTRODUCTION

The definition of biosensor, as per IUPAC is a self-containing integrated device, capable of providing specific quantitative or semi-quantitative analytical information using a biological recognition element (bioreceptor), which is in contact with the transduction element (transducer) (Fig. 1). Thus, biosensor has basically two components [1,2]. First, a biological recognition element also termed as capture probe can be a complementary DNA, enzyme (or substrate), antigen (or antibody), or a receptor protein. The recognition element is highly selective to the target analyte to be identified and therefore confers high selectivity to the biosensor in comparison with other chemical sensors. The second component of biosensor is a transduction element (optical, mass, electrical, or electrochemical), which converts the analyte concentration into a measurable electrical signal. The high sensitivity, specificity, reusability, label-free, and compact size of biosensor makes them attractive alternatives to conventional analysis techniques [3]. The major applications of biosensor is in medical field for the diagnosis of different diseases, for example, cancer detection, blood glucose monitoring in case of diabetic patients, drug discovery, drug analysis, and whole blood analysis. Furthermore, biosensors have also found applications in food technology, environmental monitoring, industrial process control, and homeland security [4]. According to the science direct, using the keyword “biosensor” around 7000 papers have been published in the year 2016.

The advancement in the nanotechnology has led to the development of several highly sensitive sensing platforms, which can detect a very low concentration of specific target analyte. Among the most promising platforms, nanostructured porous silicon (PSi) has been extensively studied as a detection

Corresponding author: N.H. Maniya, e-mail: nalinmaniya@gmail.com and nalinmaniya@csmcri.res.in

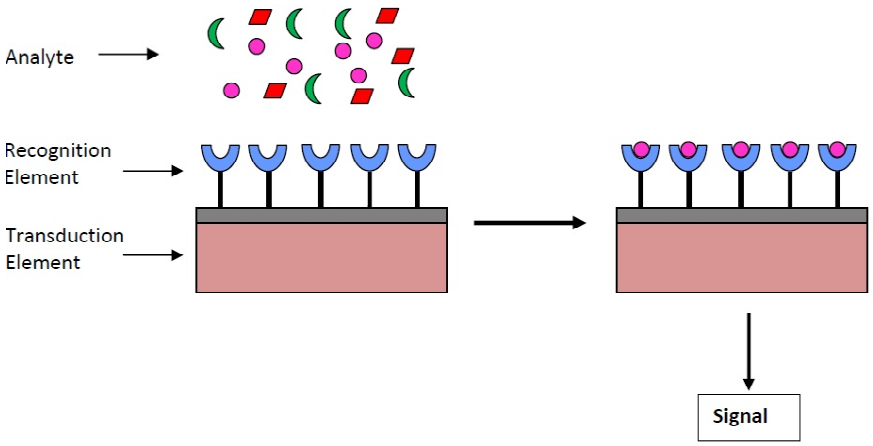

Fig. 1. Schematic diagram of biosensor consisting of a recognition and transduction elements.

platform for different biomolecules mainly due to its unique physical and optical properties. The tremendous interest in PSi as biomaterial was developed after the discovery of photoluminescence from PSi by Leigh Canham in 1990s [5], though PSi was first discovered in 1956 by Uhlir [6]. Uhlir found porous surface on a silicon substrate while conducting his experiments on silicon wafers by electrochemical method. Then, canham also demonstrated that PSi is biocompatible, biodegradable, and non-toxic biomaterial [7-9]. Thereafter, different PSi single and multilayer structures have been prepared for a numerous biomedical applications such as chemical and biosensing [10-20], bioimaging [21,22], biomolecular screening [23], tissue engineering [24], and drug delivery [25-28]. An important properties of PSi for biosensing are its unique physicochemical and optical properties such as easy top-down fabrication by electrochemical etching using silicon wafer; the surface of PSi can be easily stabilized and functionalized with biomolecules; PSi can be prepared in the form of single layer and double layer interferometer, distributed Bragg reflector, microcavity, rugate filter, waveguide, Bloch surface wave, and ring resonator structures to improve the sensitivity of the optical measurement; a very high surface area per volume of porous matrix allows the higher degree of immobilization of capture probe, which helps in miniaturization of sensor; PSi is biocompatible and biodegradable, which is useful for *in vivo* biosensing; PSi is also compatible with microelectronics and MEMS fabrication systems [11,29-38]. PSi biosensor also allows real-time monitoring of target analyte by measuring the optical properties. Furthermore, PSi biosensor can be placed inside the human body as implantable device because PSi is biocompatible and degrades into non-toxic orthosilicic acid, which can be excreted through the urine [39-42].

PSi optical biosensor has been already exploited for the detection of DNA [13,43-46], antibody [47-50], enzyme [36,51,52], whole bacterial and yeast cell [53-55], virus [56,57], protein, and other small analytes [41,58-62] by immobilizing the corresponding capture probe on a surface. When a target analyte binds with capture probe on the PSi, a change in the average refractive index of the PSi layer occurs and this causes the shift in the wavelength of the characteristic spectral peak.

First section of the review covers the PSi fabrication methods including electrochemical etching and stain etching for the development of different single and multilayer PSi optical structures. A second and third section focuses on PSi micro and nanoparticles preparation for *in vivo* biosensing with emphasis on PSi biocompatibility. Surface stabilization and functionalization strategies and immobilization procedures for an attachment of biomolecules on PSi are highlighted in the fourth and fifth sections. Then, in sixth section, detection of different biomolecules by PSi optical biosensor is rigorously reviewed with regards to the recent developments and with a special focus on *in vivo* and PSi photonic particles biosensing.

2. FABRICATION OF PSi

2.1. Electrochemical etching

The most widely used method for PSi fabrication is an electrochemical etching using silicon wafers and hydrofluoric acid (HF) based electrolytes [6]. In addition to electrochemical etching method, PSi is fabricated less frequently by several other methods such as stain etching [63,64], metal-assisted chemi-

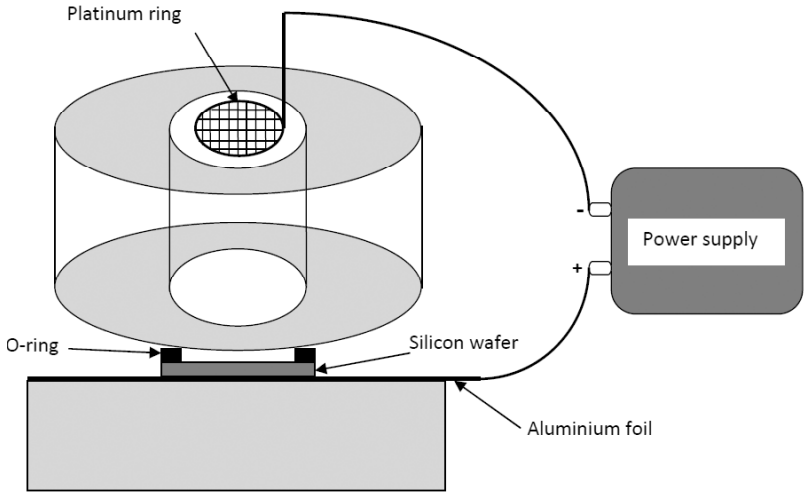

Fig. 2. Schematic diagram of etching cell used for PSi formation by electrochemical etching.

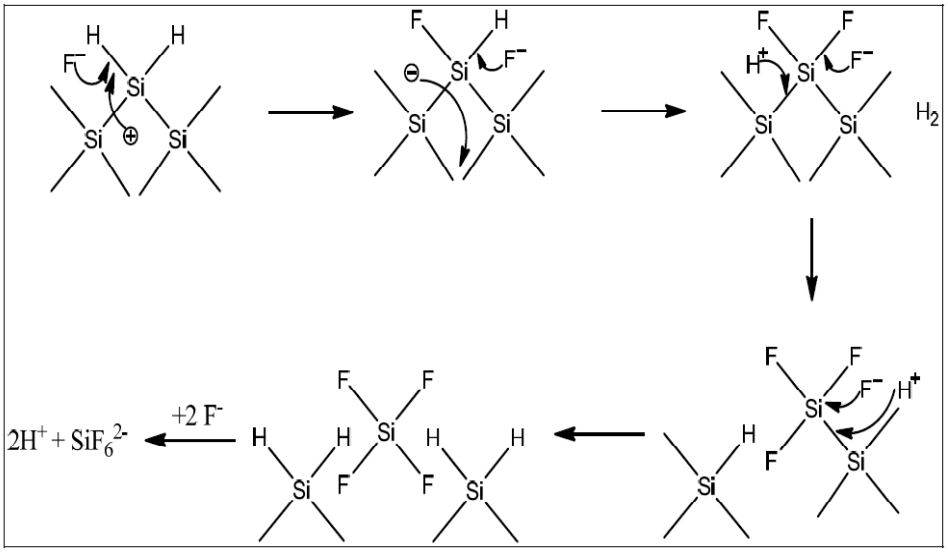

Fig. 3. Mechanism of silicon dissolution by HF during electrochemical etching.

cal etching [65,66], photochemical etching [67,68], gas, vapour, and spark induced etching [69-71]. The two major advantages of electrochemical method than the other fabrication methods are the possibility of preparing PSi multilayer structures, for example, microcavity and reproducible fabrication of porous layer with controlled physical and optical properties [72]. In order to fabricate PSi, silicon wafers with either boron doped (p-type) or phosphorus doped (n-type) and different dopant concentration is used. Immediately before etching, silicon wafers are dipped in a chemical solution to remove the organic residues present on the silicon surface. The electrochemical etching of silicon wafer is performed in the etching cell, which is generally made up of acid resistant material such as Teflon using two electrode configuration under galvanostatic control (Fig. 2). In this method, HF based electrolytes are filled into the etching cell and a current is applied between the anode, which is silicon wafer and a cathode (usually made of platinum) [73]. In order to reduce the formation of hydrogen bubbles, to improve electrolyte penetration in the pores, and to prepare uniform PSi layers, ethanol is included as a surfactant in the HF based electrolytes.

Although several models have been proposed for the mechanism behind pore formation in a silicon during electrochemical etching in HF, the model proposed by Lehmann and Gosele is most widely accepted (Fig. 3) [74,75]. According this model, valence band holes are required in the initial steps for both pore formation and electropolishing [29]. For p-type silicon wafers, holes are readily available due to the boron doping while for n-type silicon wafers where holes are minority carriers, external illumination by the light source is required for the electrochemical dissolution of silicon wafer [76].

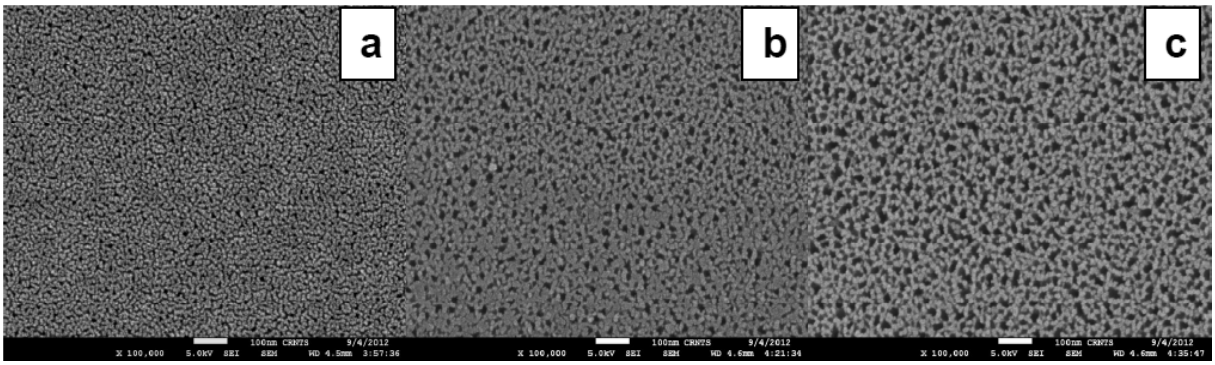

Fig. 4. Plan-view SEM images of the PSi single layers prepared with current density of (a) 10, (b) 50, and (c) 90 mA cm^{-2} for 2 min. Reprinted with permission from our work N.H. Maniya, S.R. Patel and Z.V.P. Murthy // *Superlattice.Microst.* **55** (2013) 144. (c) 2013 Elsevier.

As shown in Fig. 3, during electrochemical etching, due to the applied anodic current, hole reaches hydrogen-terminated surface of silicon and a nucleophilic attack of the Si-H bonds by fluoride ions takes place resulting in the formation of Si-F bond. The formed Si-F bond exerts a polarising influence resulting in another F^- ion bonds to the silicon with the generation of H_2 molecule and the injection of one electron into the electrode. Subsequently, polarization induced by the two Si-F bonds weakens the Si-Si backbonds that are easily attacked by HF or H_2O in presence of a second hole, in a way that the silicon surface atoms remain bonded to fluoride atoms. The unstable silicon tetrafluoride (SiF_4) molecule reacts with two HF molecules in a solution to form highly stable H_2SiF_6, Eq. (1). In this way, silicon atom is removed from the surface resulting in an atomic size dip in the surface. This process of pore formation continues till there are enough availability of electrolytes, holes, and anodic current. A net reaction for pore formation in silicon wafer is given in Eq. (1), where 'h' refers to the valance band holes.

$$Si + 2h^+ + 6HF \rightarrow H_2SiF_6 + H_2 + 2H^+ . \quad (1)$$

Porous layer with pores of different sizes, for example, micropores (< 2 nm), mesopores (2-50 nm), and macropores (> 50 nm) can be prepared in the silicon wafer. By varying current density, electrolyte concentration, type and concentration of dopant (p-type or n-type), and crystalline orientation of silicon wafer, pores with varied diameters ranging from 1 nm to few microns and smooth walled or branched, interconnected or independent can be easily prepared [29]. Pore size of PSi is highly dependent on the applied current density. As shown in Fig. 4, different pore diameters can be prepared by varying current densities. For current density of 10 mA cm^{-2}, a small pore diameter of 9.29 nm and at higher current density of 90 mA cm^{-2}, larger pore diameter of 24.75 nm was obtained (Figs. 4a and 4c) [72]. The pore diameter of 18.23 nm was observed for current density at 50 mA cm^{-2} (Fig. 4b). For p-type silicon wafer, pore size increases with increase in the current density and decrease in HF concentration [77]. However, in the case of n-type silicon, pore diameter also depends on illumination parameters such as wavelength of illumination and intensity in addition to the current density [78,79]. In a both p-type and n-type wafers, pore size increases with an increase in dopant concentration and decrease in resistivity. Furthermore, type of dopant also affects pore diameter as n-type silicon gives larger pores than p-type silicon [80].

The porosity and thickness of PSi are two most important properties, which determine the optical properties and immobilization capacity of PSi sensor. Porosity of PSi is represented as a ratio of total pore volume to the total volume. It has been established that the porosity and thickness of porous layer increases with an increase in current density and etching time, respectively [72]. Porosity can be increased from 5 to 95% by increasing current density. This is very advantageous for the preparation of multilayer structures such as Bragg reflector, microcavity, and rugate filter where a change in current density results in change in porosity of different layers. PSi optical biosensor with large pore sizes in upper layer and small pore sizes in lower layer can be fabricated so that enzymes and other large molecules retain in the upper layer and a reaction product to be identified only enters into a lower layer. This is of high importance for a label-free quantification of enzyme kinetics in a real-time. Additionally, for *in vivo* biosensing applications, degradation rate of porous matrix in aqueous media is dependent on a porosity and pore size of layer [81]. PSi with small pores yield large surface area and

degrades easily than large pores with low surface area.

Surface area of PSi can be varied from few m^2/g to 1000 m^2/g by changing the etching parameters. PSi surface area is found to be increased with increase in HF concentration and decreased with increase in current density and etching time. The resistivity of silicon wafer also influences surface area with decrease in surface area is observed by decreasing the resistivity [77]. Freshly etched PSi is mostly covered by different hydride species (Si-H, Si-H_2, and Si-H_3) and surface stabilized by different methods which can be investigated by Fourier transform infrared spectroscopy. A specific surface area of PSi, which is a accessible area of solid volume per unit of volume can be estimated by gas adsorption measurements. The morphology of prepared PSi, for example, porosity, pore size, and thickness can be easily characterized by several destructive and non-destructive methods. The porosity and thickness of PSi film can be obtained by destructive gravimetric method [73]. In this method, weights of PSi sample before etch, after etch, and after dissolving porous layer in basic aqueous solutions (KOH or NaOH) are used to determine porosity and thickness, Eqs. (2) and (3).

$$P = \frac{m_1 - m_2}{m_1 - m_3}, \tag{2}$$

$$W = \frac{m_1 - m_2}{A\delta_{Si}}, \tag{3}$$

where m_1 is weight of silicon sample before etch, m_2 is weight after etch, m_3 is weight after dissolving porous layer in a basic aqueous solution, A is exposed wafer area to HF electrolyte during etching, and δ_{Si} is the density of silicon.

2.2. Stain etching

Stain etching is the second most accepted PSi fabrication method after electrochemical etching and used commercially for the preparation of PSi powders. It is used for the preparation of PSi from silicon powders or other forms in which electric power cannot be supplied. In stain etching, cathodic reaction between HF and nitric acid produces NO (nitric oxide), which serves as a hole injector in the silicon surface and make brownish or reddish color PSi film without any external electric power supply [63,64]. Although stain etching is a simple method than electrochemical etching due to the no requirement of power supply, it is less frequently used to prepare PSi due to the less reproducibility and non-fabrication of multilayer structures.

2.3. Metal-assisted chemical etching

Metal-assisted chemical etching has shown increasing attention in recent years for the fabrication of PSi structures for optical biosensing application. In this method, noble metals such as Ag, Au, Pt or Au/Pd is deposited onto the silicon substrate prior to the etching process. The metal catalyses the dissolution of silicon, when metal-decorated silicon substrate is immersed in a solution composed of HF and H_2O_2 forming PSi micro and nanostructures. During the reaction, valence band holes are injected into the silicon substrate by means of the decomposition of H_2O_2 on a metal surface, which causes the etching reaction to be localized in the vicinity of the metal. Porosity of the resulting PSi structures can be controlled by adjusting the composition of etching solution [65,66].

2.4. Optical structures of PSi

Different optical structures of PSi can be fabricated such as single layer and double layer interferometer, Bragg mirror, microcavity, rugate filter, waveguide, Bloch surface wave, and ring resonator for the development of biosensor (Fig. 5). PSi single layer is fabricated by different methods such as electrochemical etching, stain etching, and metal-assisted chemical etching (Fig. 5a). In electrochemical etching, which is most commonly used technique for single layer preparation, a single constant current density is applied for the fabrication. Thickness of single layer is strongly dependent on the etching time. In addition, other physical properties, for example, porosity, pore size, surface area are varied according to current density, etching time, electrolyte composition and pH, type and level of doping in silicon wafer, resistivity, and crystallographic orientation.

PSi double layer is fabricated by changing the current density during etching process. Since the new pore formation occurs at the bottom of porous layer i.e. at crystalline silicon surface, a change in current density results in change in porosity and formation of new layer beneath the first layer (Fig. 5b). This excellent property of PSi allows for the fabrication of complex multilayer structures. PSi single and double layer structures display significant series of interference fringes in the reflectance spectra and this type of Fabry-Perot fringe pattern results from the constructive and destructive inter-

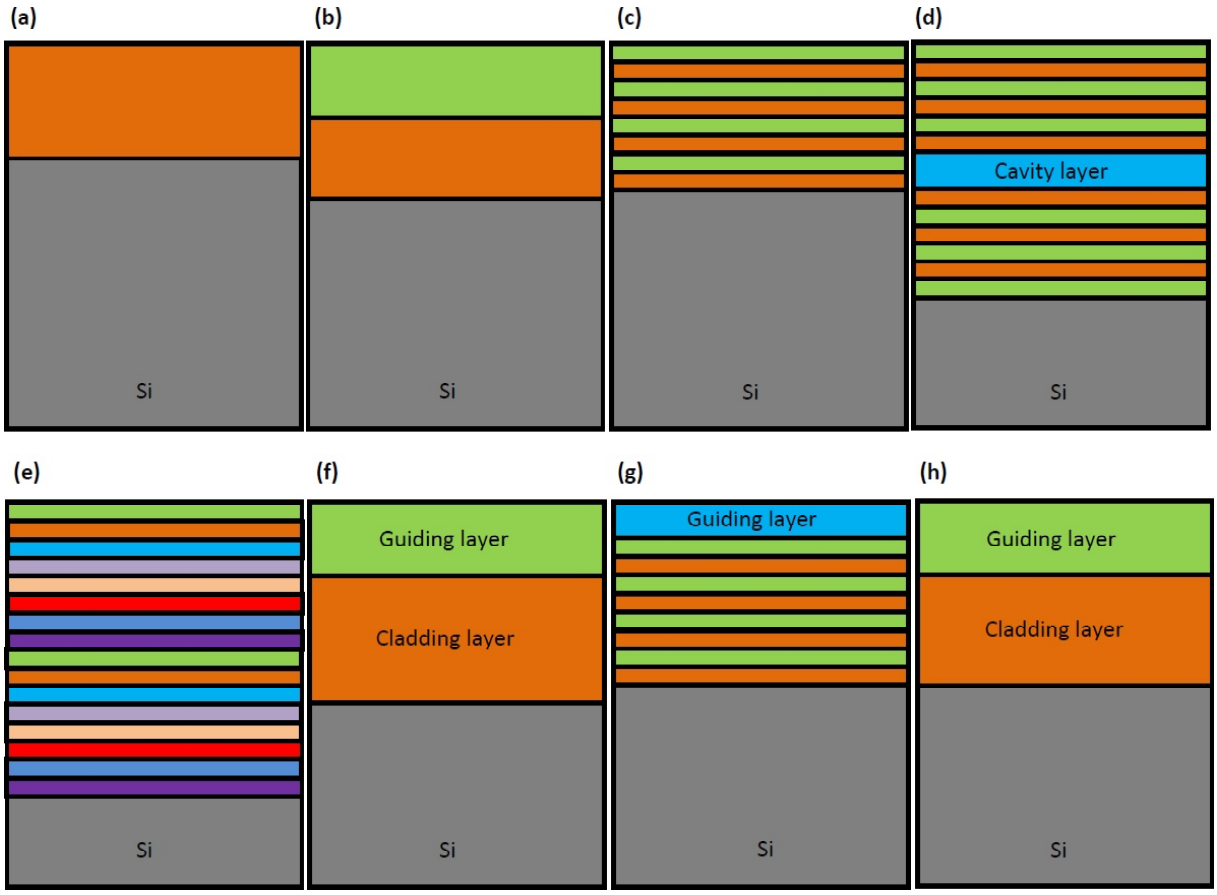

Fig. 5. Schematics of the various PSi optical structures: (a) single layer, (b) double layer, (c) Bragg reflector, (d) microcavity, (e) rugate filter, (f) waveguide, (g) Bloch surface wave, and (h) ring resonator.

ference of light reflected from the PSi-medium and PSi-crystalline silicon interfaces. The change in interference fringes is observed due to the change in refractive index when the target analyte binds on a single or double layer PSi optical biosensor. The maxima in a fringe pattern (λ_{max}) is related to the physical properties of PSi by the equation (Eq. (4) [13].

$$m\lambda_{max} = 2nL, \tag{4}$$

where m is a spectral order, n is average refractive index of the layer, L is the thickness of PSi layer, and term $2nL$ is also referred as effective optical thickness (EOT).

PSi distributed Bragg reflector (DBR) is one dimensional (1D) photonic structure in which discrete layers of two different refractive indices and thicknesses are staked alternately (Fig. 5c). This photonic structure with alternating layers gives photonic bandgap (PBG) centred at λ where rejection of a wide range of wavelengths of light is observed. To design DBR, each discrete layer should have optical thickness (i.e., nL) of one quarter of design wavelength (λ) and the constituent layers must be phase-matched, Eq. (5) [82].

$$\lambda / 4 = n_1 L_1 = n_2 L_2, \tag{5}$$

where n_1 and n_2 are the refractive indices, L_1 and L_2 are thicknesses of two discrete layers and λ is the Bragg wavelength corresponding to the centre of PBG region [33]. The full-width at half-maximum (FWHM) bandwidth of a PBG can be calculated based on the refractive indices of the constituent layers using following equation:

$$\Delta\lambda / \lambda = \frac{4(n_1 - n_2)}{\pi(n_1 + n_2)}, \tag{6}$$

where n_1 and n_2 are the refractive indices of high and low index layers, respectively, and λ is the centre wavelength of PBG.

PSi microcavity is another important multilayer photonic structure composed of two distributed Bragg reflectors with an active layer (of $\lambda/2$ optical thickness) in the middle of the structure (Fig. 5d) [83]. The distinguishing feature of microcavity is the narrow resonance peak that appears in the reflectance spectrum. A change in resonance peak or cavity position in the reflectance spectrum occurs when a molecule is attached to the internal surface

of the PSi microcavity biosensor [84,85]. The quality factor (Q) of microcavity is defined as:

$$Q = \lambda / \Delta\lambda, \quad (7)$$

where λ is the resonant wavelength and $\Delta\lambda$ is the FWHM of the resonance. If the Q value is higher, light is more efficiently confined inside the cavity and sharper the resonant dip is observed. The increase in reflectance of the Bragg mirrors causes an increase in Q value.

PSi rugate filter is also 1D photonic structure in which porosity and in turn refractive index varies smoothly and periodically in depth (Fig. 5e) [86]. Similar to DBR, rugate filter also shows a PBG in the reflectance spectra, however, slightly narrower than the bandwidth of a quarter-wave stack. Furthermore, higher order harmonics can be completely eliminated in a rugate filter [87]. The refractive index profile $n(x)$ of a rugate filter centered on λ_0 can be written in the following form:

$$n(x) = n_0 + \Delta n / 2 \sin(4\pi x / \lambda_0), \quad (8)$$

where x is a perpendicular distance into the plane of filter, n_0 is average refractive index, and Δn is refractive index contrast. The particles of PSi rugate filter called “smart dust” are also developed for detection of biomolecules and organic vapour [88-91].

Recently, new PSi structures including waveguide, ring resonator, and Bloch surface wave have been developed for the biosensing and several other applications. PSi optical waveguides have been exploited for applications ranging from optoelectronics to chemical and biosensors. Unlike many other optical structures such as Bragg mirror, rugate filter, and microcavity, light incident on a waveguide can couple into a propagating in-plane mode under the proper excitation conditions. A waveguide structure consists of high refractive index layer (guiding layer) surrounded by a lower refractive index media (cladding layers) (Fig. 5f). PSi single layer, double layer, or triple layer structures has been fabricated to achieve PSi waveguides [45]. Prism, grating, and butt coupling configurations are commonly used to couple light into the PSi waveguide. In PSi waveguide structure, light is strongly confined in the top waveguiding layer by total internal reflection. PSi waveguide allows the detection of biomolecules on the guiding layer itself whereas other structures such as microcavity detect the biomolecules when the analyte reaches the cavity layer. Therefore, faster response and less sample volume requirement is achievable with PSi waveguide [92,93].

PSi photonic structures supporting resonantly coupled optical Bloch surface waves have been developed for the detection of biomolecules. PSi Bloch surface wave structures have been prepared for simultaneous detection of small chemical molecules and bacteriophage [57]. PSi Bloch surface wave is composed of periodic multilayer with an alternating refractive indices like Bragg reflector and an aperiodic outermost layer as the surface wave guiding layer (Fig. 5g). The detection of biomolecules occurs on the surface wave guiding layer. The coupling configurations similar to a waveguide are used for PSi Bloch surface wave structures. Bloch surface wave has advantages similar to a waveguide, for example, fast sensor response and less analyte volume required in comparison to other structures because the sensing element present on the top layer. Also, lower detection limit can be obtained by accurately measuring small spectral shifts due to the narrower spectral features of resonant modes [36,94].

To prepare ring resonator, PSi slab waveguides are fabricated by electrochemical etching of silicon wafers. PSi slab waveguide contains guiding layer and cladding layer, which are fabricated at two different current densities. Electron beam lithography and reactive ion etching are then used to pattern rings on the slab waveguides (Fig. 5h) [43,60]. The Q factor for ring resonator is defined as:

$$Q = \frac{\lambda_{res}}{FWHM}, \quad (9)$$

where λ_{res} is the resonance wavelength.

3. MICRO AND NANOPARTICLES OF PSi

A novel and unique properties arise at micro and nanoparticulate dimension due to the reduced micro or nanoscopic size and large surface area than its bulk material. A simple preparation method for PSi micro and nanoparticles resulted in a number of applications in biosensing, bioimaging, and drug delivery. PSi particles have following interesting physicochemical properties, which can be used for *in vivo* applications. For example, PSi particles prepared from single or multilayer structures retain its optical properties and can be used for label-free sensing. Surface of particles can be easily chemically modified for the stability and immobilization of biomolecules. Additionally, PSi is found to be nontoxic or very less toxic in biological system, and therefore it can be an excellent biomaterial for *in*

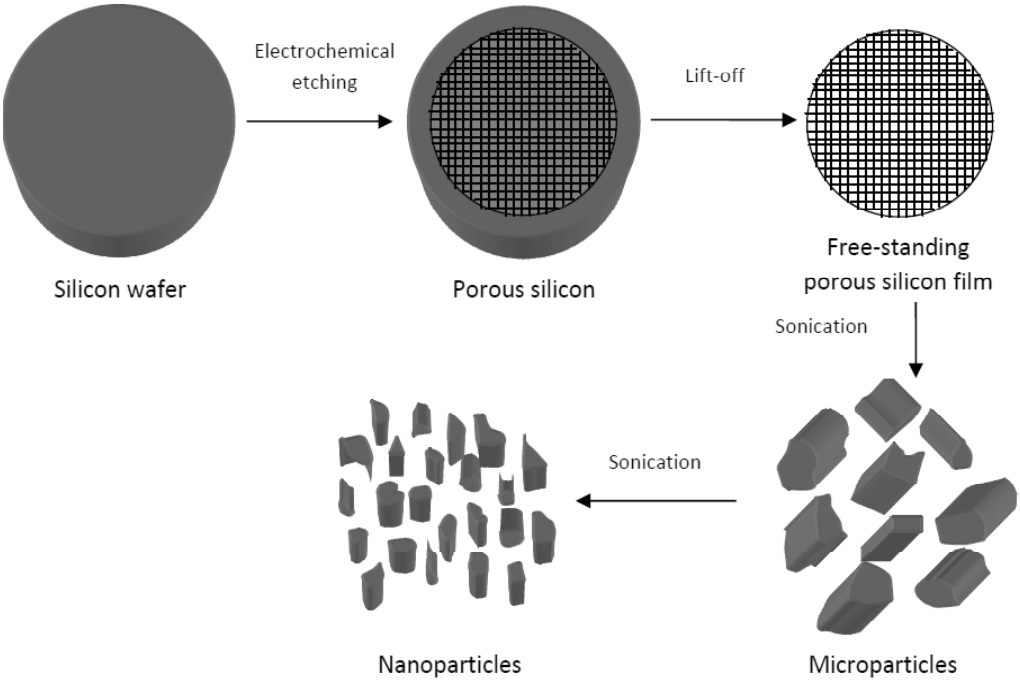

Fig. 6. Schematic diagram of PSi micro and nanoparticles preparation by ultrasonic fracture of freestanding films.

vivo applications. During electrochemical etching, based on etching time, a thin film of PSi is fabricated on bulk silicon substrate. Hence, in order to prepare PSi particles, thin film must be detached from the silicon substrate. PSi film is removed by electropolishing (lift-off) process by applying current density for several seconds and using low concentration of HF. In this process, etching current surpasses the rate at which fluoride ions transported to the pore tips due to the low concentration of HF resulting in the formation of oxide layer (SiO_2) instead of silicon dissolution (SiF_4). The oxide layer then dissolves in HF and PSi film detaches from silicon wafer [29].

PSi micro and nanoparticles are then prepared by fractionation of the freestanding films using ultrasonication, ball milling, or jet milling. In ultrasonication, PSi films are placed in ethanol or other solvent and sonicated in ultrasonic bath for several minutes to hours for the preparation of micro and nanoparticles, respectively (Fig. 6) [95,96]. The size of particles depends on the solvent used and time duration for which ultrasonic waves applied. Ultrasonication is a simple and less expensive process, but produces particles of irregular shape and wide size distributions from tens of nanometers to several micrometers. However, specific sized particles can be obtained by either filtration or centrifugation of ultrasonic fractured particles. In a recent study, uniform sized PSi nanoparticles have been prepared by introducing high porosity layers in a regular porosity layers followed by ultrasonic fracture [97,98]. The other expensive alternatives to prepare particles with uniform shape are lithography and microdroplet patterning methods [99,100].

4. BIOCOMPATIBILITY, BIODEGRADABILITY, AND TOXICITY OF PSi

Micro and nanoengineered materials should be biocompatible, non-toxic, non-immunogenic and biodegradable. Biocompatibility, biodegradability, and toxicity are the most important properties of any nanomaterials, treatments and devices, which decide its suitability for human use. In 1990s, Canham carried out first *in vitro* studies on biocompatibility of PSi using microporous, mesoporous and macroporous structures in the simulated body fluid [7]. Then, a number of studies addressing *in vitro* and *in vivo* biocompatibility of PSi such as calcification [7-9], cell adhesion [101,102], protein binding [103], and tissue biocompatibility [104] has been carried out. PSi is an excellent biomaterial for biomedical applications owing to its biocompatibility, biodegradability, low toxicity and solubility. PSi is a bioinert material and has shown good biocompatibility in biological systems without interrupting normal cellular functions.

Moreover, PSi has been found to be a biodegradable material, which dissolves in biological fluids. PSi degrades into a non-toxic orthosilicic acid ($Si(OH)_4$), which is a natural form of silicon in our bloodstream and tissues and can be absorbed by the human body or excess readily excreted by kidneys [40,105,106]. In addition, PSi has been found to support growth of several cell types including osteoblasts, neurons, and hepatocytes [24,107,108]. The hydrolytic dissolution of a silicon surface occurs as represented in following equations, see Eqs. (10), (11), and (12):

$$SiH_4 + 2H_2O \rightarrow SiO_2 + 4H_2, \quad (10)$$

$$Si + O_2 \rightarrow SiO_2, \quad (11)$$

$$SiO_2 + 2H_2O \rightarrow Si(OH)_4, \quad (12)$$

In vitro and *in vivo* biocompatibility and cytotoxicity studies of PSi have been performed for different parameters like size, shape, surface chemistry of nanomaterials, dosage size, and time of exposure using different cell types and animal models. The *in vitro* and *in vivo* biocompatibility of thermally oxidized and aminosilanized PSi membranes, has been carried in the human ocular cells and rat eye. Both PSi membranes supported a growth of human lens epithelial cells *in vitro* on its surface. When membranes were implanted under the conjunctiva of normal rat eye, no erosion of the surrounding tissue, inflammatory response, or vascularisation was observed. In addition, human ocular cells supported by PSi membranes were able to survive, divide, and migrate into ocular tissue spaces *in vivo* [106].

A correlation between surface chemistry, particle size, concentration of PSi microparticles, and *in vitro* cytotoxicity has been also established using human colon carcinoma (Caco-2) cells [109]. PSi particles of different size ranges, surface chemistries, and concentrations were prepared. Smaller particles of size range of 1.2-25 μm showed higher cytotoxicity in comparison to larger particles. For particle sizes >25 μm, non-toxic threshold for particle concentration was found to be <2 mg mL^{-1} for thermally hydrocarbonized and carbonized PSi particles and <4 mg mL^{-1} for thermally oxidized PSi microparticles. Furthermore, thermally oxidized PSi was found to be less cytotoxic than thermally carbonized or hydrocarbonized PSi. This variation in toxicity is owing to the hydrophilic surface and no significant reactive oxygen species (ROS) production in the cells by thermally oxidized PSi whereas ROS production in the cells by thermally carbonized PSi and ATP depletion in the cells by hydrocarbonized PSi microparticles [109].

The biocompatibility of positively and negatively charged thermally oxidized and carbonized PSi microparticles in human corneal epithelial and retinal pigment epithelial cells with the possibility of applications in the eye has been studied [110]. PSi with two different particle sizes of 25-53 and 53-75 μm and different surface chemistries were prepared. Both the particle sizes were equally well tolerated when administered into the epithelial cells especially at concentrations lower than 200 μg mL^{-1} and the toxicity of PSi particles was found to be concentration dependent. In addition, positively charged amino grafted thermally oxidized and carbonized PSi microparticles were better tolerated than negatively charged non-grafted particles even at higher concentrations. Also, positively charged amino grafted particles gave an additional advantage of closer contact with the negative cell membrane to promote cell adhesion. Nieto et al. [111] has also demonstrated good biocompatibility of fresh and thermally oxidized PSi microparticles in the rabbit eye.

The evaluation of *in vitro* and *in vivo* impact of PSi nanoparticles on immune cells and human red blood cells (RBCs) has been investigated recently [112]. Following five different types of PSi nanoparticles, namely thermally oxidized PSi (TOPSi), thermally carbonized PSi (TCPSi), (3-Aminopropyl) triethoxysilane functionalized thermally carbonized PSi (APSTCPSi), thermally hydrocarbonized PSi (THCPSi) and undecylenic acid functionalized THPSi (UnTHCPSi) with similar size, surface area and pore volume were prepared. The toxicity rank order of PSi nanoparticles was found to be: APSTCPSi > UnTHCPSi > THCPSi > TCPSi ≈ TOPSi. Also, it was established that different PSi nanoparticles can trigger various toxicity mechanisms in different cells. Based on toxicity analysis on different cells, the concentration and time dependent toxicity was observed in the following order: T-cells > monocytes > macrophages > B-cells. Therefore, toxicity of PSi nanoparticles varied depending on cell line characteristics such as doubling time, metabolic activity, growth pattern, and type of nanomaterial in contact with them. In case of effect of nanoparticles on RBC, a significant correlation like immune cells was observed between surface chemistry, amount of PSi nanoparticles adsorbed on the cell surface, and the extent of morphological changes.

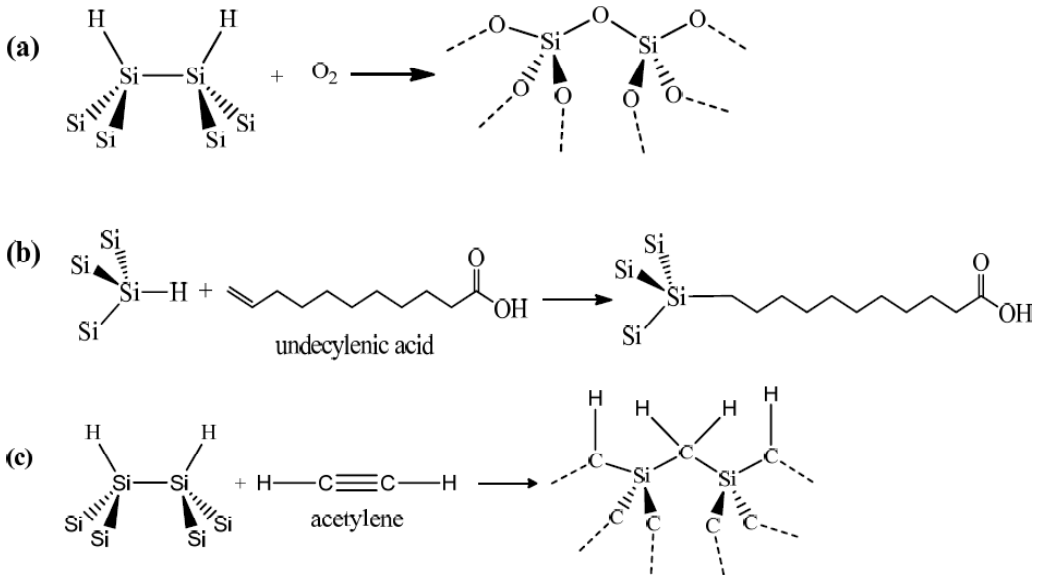

Scheme 1. Surface modification of the hydrogen-terminated (Si-H) surface of PSi by (a) thermal oxidation, (b) thermal hydrosilylation using undecylenic acid, and (c) thermal carbonization using acetylene.

5. CHEMICAL MODIFICATION OF PSi

Surface chemistry plays an important role in stability, immobilization of biomolecules, and degradation of PSi matrix. Freshly etched PSi surface is highly reactive and unstable due to the hydride terminated (Si-H, Si-H_2, and Si-H_3) groups and slowly aged in ambient air, thereby affects both its physicochemical and optoelectronic properties. Depending on environmental conditions such as temperature, humidity, and air composition, aging of native PSi occurs due to the oxidation of surface [113]. Different impurities, for example, oxygen, carbon, and fluorine are also observed shortly after PSi fabrication. Furthermore, sample for biosensing contains either water or other liquid medium, which may further oxidize, degrade or react with the PSi surface. Therefore, chemical modification of native surface is required to stop aging and to further stabilize the PSi. The three most extensively used treatments for stabilization and surface modification of PSi are oxidation, hydrosilylation, and thermal carbonization.

5.1. Oxidation of PSi

PSi oxidation is most commonly used for the stabilization of PSi surface for biosensor, drug delivery, and several other applications. Oxidation not only stabilizes the surface but also converts hydrophobic surface of native PSi into hydrophilic, which allows water to effectively infiltrate the pores. PSi oxidation can be carried out by thermal, photo, anodic, and chemical methods. In order to perform oxidation, different organic and inorganic agents such as hydrogen peroxide, ozone, dimethyl sulfoxide, and pyridine have been used [31,114,115]. Among the all oxidation methods, thermal oxidation is simplest method to stabilize PSi surface (Scheme 1a). Partially thermally oxidized surface can be obtained by heating PSi in air at 300 °C for few hours and completely oxidized surface by heating at 900 °C. A partial oxidation incorporates oxygen into the Si-Si bonds resulting in the formation of backbonded species. However, as oxidation temperature increases, these backbonded species gradually diminish and completely removed by oxidation at 600 °C [96,116]. The time required for complete thermal oxidation depends on the thickness and type of PSi sample, for example, microporous oxidizes within an hour and mesoporous requires 3 hours whereas macroporous silicon oxidizes after 12 hours. The disadvantage of thermal oxidation is decrease in the pore diameter, porosity, and specific surface area due to the structural expansion.

5.2. Hydrosilylation of PSi

Hydrosilylation of PSi is performed by thermal, photochemical, or Lewis acid catalysts via the reaction of native surface Si-H species with alkenes, alkynes, or aldehydes [30,117-122]. In hydrosilylation reaction, Si-H bond is replaced with Si-C bond that increases the stability of surface and allows an attachment of range of diverse functional groups for applications in drug delivery [123,124], chemical sensors [125], and biosensors [36,126,127]. Si-C

surface has higher kinetic stability due to low electronegativity of carbon in comparison to Si-O surface produced by oxidation.

Thermal hydrosilylation is most frequently used among other hydrosilylation methods where hydrogen-terminated PSi is immersed in a neat alkene and microwave radiation is applied [117,118]. This method commonly referred as microwave-assisted hydrosilylation not only provides a stable Si-C surface, but also allows the introduction of a wide variety of functional groups on a PSi surface. In this hydrosilylation reaction, very high treatment efficiency and a higher surface coverage can be obtained due to the high energy of microwaves [119]. Moreover, like thermal oxidation, hydrophilic surface can be prepared by reaction of undecylenic acid with PSi for biosensor preparation (Scheme 1b). Freshly etched PSi should only be used for hydrosilylation because reaction takes place between Si-H groups and terminal alkene. PSi hydrosilylation have been performed by utilizing different organic compounds including undecylenic acid, dodecene, methoxy, trimethylsiloxy, and folate [36,118,119,127-130].

PSi surface modifications can also be performed by chemical or electrochemical grafting techniques using Grignard, alkyl, or aryllithium reagents [131-134]. Electrochemical oxidation of methyl-Grignards and electrochemical reduction of phenyldiazonium salts have been used for the preparation of dense monolayers covalently attached to the PSi and single crystal silicon, respectively [135,136]. The stability of PSi surface can also be improved by using organohalides, which produces Si-C bonds by the cleavage of Si-H bonds due to the electrochemical reduction [137]. Grafting technique is a substitute to hydrosilylation but it also allows attachment of methyl group, which is not possible with the hydrosilylation. Both grafting and hydrosilylation techniques make stable Si-C surface with coverage of 20-80%, which means Si-H groups still remain on a surface after the reaction. Si-H groups has been completely removed by methylation using CH_3I on the functionalized surface to form a completely Si-C terminated surface [138].

5.3. Thermal carbonization of PSi

PSi thermal carbonizations have been extensively investigated by Salonen and coworkers since year 2000 [139-141]. The major advantages of this method are very high surface coverage and more stable Si-C surface than the surface produced by thermal oxidation. A stable Si-O surface is produced by thermal oxidation but the Si-O bonds are vulnerable to hydrolytic attack in aqueous solutions. On the contrary, thermal carbonization produces Si-C surface, which is stable in a humid atmospheres and even in very harsh chemical environments [142].

Thermal carbonization of PSi is performed using acetylene vapour to make carbonized or hydrocarbonized PSi (Scheme 1c). In this process first acetylene vapour is flushed and then thermal treatment is done. Here two different types of surface terminations can be obtained depending on the temperature in thermal treatment. First type is thermally hydrocarbonized PSi, which is produced by constant flow of acetylene and nitrogen gas followed by heating at temperature below 700 °C. The produced surface is hydrophobic due to presence of some Si-H species still on a surface. Second type of surface termination is completely carbonized PSi, which can be formed by heating at temperature above 700 °C after acetylene flow stopped. This PSi surface is highly stable in acidic as well as basic solutions and inert in chemically harsh environments [143]. The high stability is extremely advantageous for the functionalization of biomolecules and implantable biosensor development. In addition to that thermal carbonization of PSi results in lesser decrease in surface area in comparison to thermal oxidation. However, thermally oxidized PSi without any chemical species is less likely to produce any toxic side effects than the thermally hydrosilylated or thermally carbonized PSi. But thermally hydrosilylated or thermally carbonized PSi is preferred when long term or extended biosensing is required as in case of implantable devices.

6. DERIVATIZATION AND BIOFUNCTIONALIZATION OF PSi

After the surface stabilization, derivatization and biofunctionalization of PSi is carried out to immobilize biomolecules on the surface, to target PSi particles to diseased sites, and to minimize biocompatibility issues in case of *in vivo* biological applications. Oxidized PSi surface can be easily functionalized by standard silanization reactions [144]. Silane coupling agents with different terminal moieties can be attached to the PSi surface. Silanes allow stable bond formation between PSi surface and organic molecule. A coupling reagent 3-aminopropyltriethoxysilane (3-APTES) is frequently used to attach proteins, DNA, and many other biomolecules to the oxidized PSi surface (Fig. 7a) [145,146]. Both monoalkoxydimethylsilanes and trialkoxysilanes have been used for functionalization

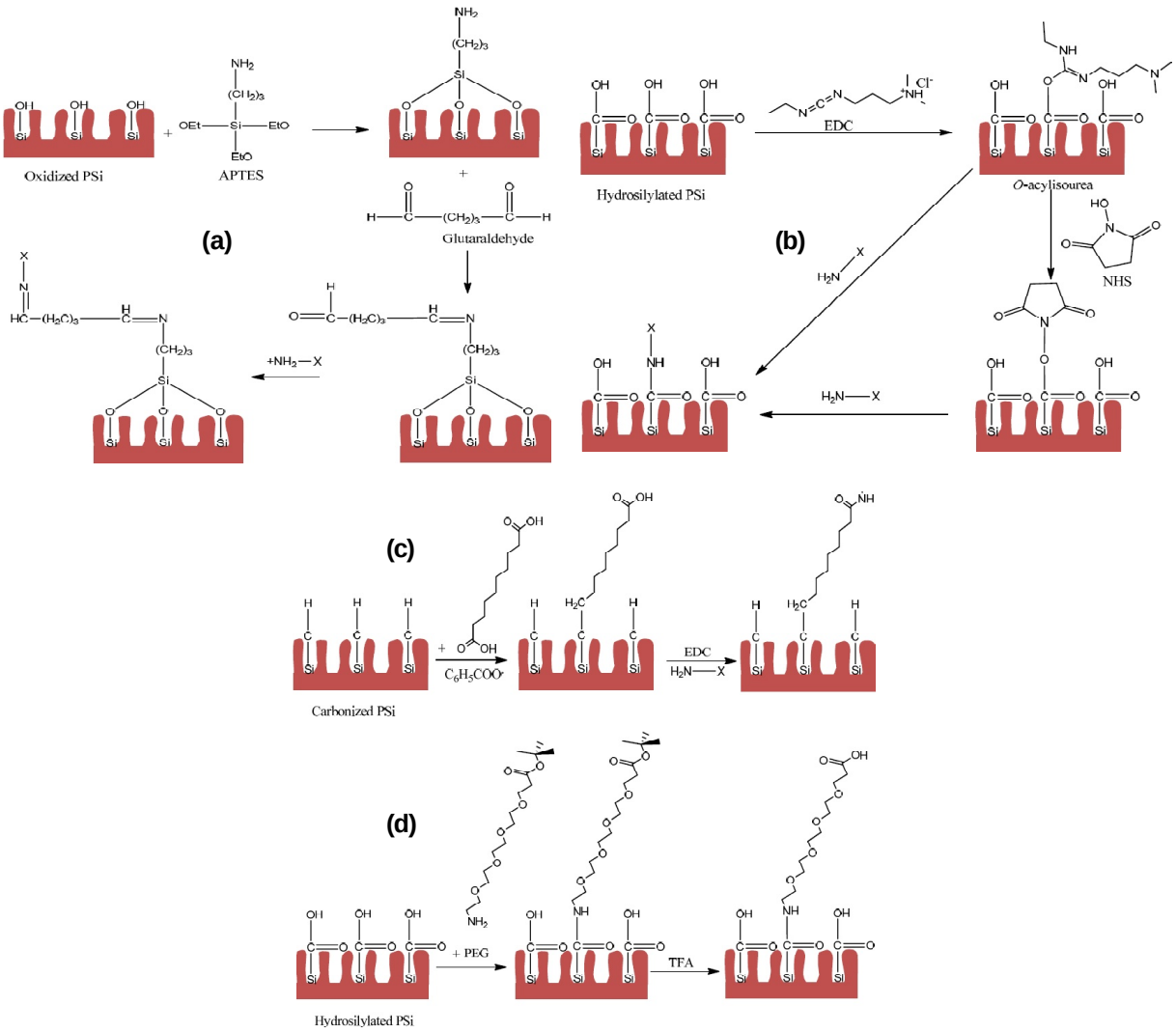

Fig. 7. Biofunctionalization of (a) oxidized PSi through APTES and glutaraldehyde chemistry, (b) hydrosilylated PSi through direct EDC and two-step EDC/NHS procedure, (c) carbonized PSi through sebacic acid followed by EDC chemistry, and (d) hydrosilylated PSi via attachment of PEG to improve biocompatibility. The reagent TFA is trifluoroacetic acid. The 'X' can be DNA, protein, or antibody, which attaches on the functionalized PSi through its amino moiety.

of PSi. However, monoalkoxydimethylsilanes is preferred over trialkoxysilanes when functionalization of microporous sample is required because trialkoxysilanes clog smaller pore openings of microporous samples [147]. The undecylenic acid attached hydrosilylated PSi surface is routinely functionalized by coupling agent 1-ethyl-3-[3-dimethylaminopropyl] carbodiimide hydrochloride (EDC) for loading of primary amine containing biomolecules [36]. As shown in Fig. 7b, EDC couples the carboxyl group of undecylenic acid modified PSi surface to the primary amine of target molecule. EDC first reacts with carboxyl group on the PSi and forms reactive intermediate (O- acylisourea), which then reacts with amine containing biomolecules through direct reaction or via N-hydroxysulfosuccinimide (NHS). Thermally carbonized PSi surface can be modified by radical coupling reaction using a linker molecule sebacic acid (Fig. 7c). The surface radicals are generated by using radical initiator benzoyl peroxide (C_6H_5COO) that reacts with sebacic acid to form hydrophilic PSi surface with carboxylic acid end. This surface can then be used for attachment of amine containing biomolecules via EDC coupling agent as displayed in Fig. 7b. Biocompatibility of stabilized PSi can be improved by attachment of polyethylene glycol (PEG) linker to the surface, which avoids non-specific binding of unwanted proteins and other interfering species (Fig. 7d) [144,146,148]. PEG linker attachment also helps in retaining sensitivity and stability of biosensor in biological systems.

Table 1. Summary of Detection of Various Biomolecules Using PSi Optical Structures (where n/d - not determined).

Analyte family	Analyte	Bioreceptor	Transducer	Detection range	Sensitivity	Response time	References
DNA	16mer target peptide nucleic acid	16 oligonucleotides	Ring resonator	500 nM	4 pm nM^{-1} (3 nM)	60 min	[43]
	15 oligonucleotides	ssDNA	Single layer	1×10^{-9}-10×10^{-9} M	1×10^{-9} M	20 min	[149]
	40 oligonucleotides	APTES,Sulfo-SMCC	Bloch surface wave	50 μM	50 μM	60 min	[94]
	24 oligonucleotides	ssDNA	Bragg reflector	200 μM	0.26 μM	2 h	[46]
Enzyme	Sortase A	Fluorogenic peptide	Microcavity	4.6×10^{-12} - 4.6×10^{-8} M	8×10^{-14} M	30 min	[150]
	Human α-thrombin	17mer Thrombin binding aptamer	Single layer	13-109 nM	1.5 nM	2 h	[153]
	Subtilisin	Gelatin	Bloch surface wave	0.37-370 nM	370 pM	20 min	[36]
	L-lactate dehydrogenase	Resazurin	Microcavity	0.16-6.5 U mL^{-1}	0.08 U mL^{-1}	10 min	[127]
	Matrix metallo-proteinases	Fluorogenic peptide	Microcavity	10^{-7}-10^{-12} M	7.5×10^{-19} M	15 min	[151]
	Matrix metallo-proteinases	Peptide	Rugate filter particles	1 nM-1.5 μM	1 nM	24 h	[90]
	Horseradish peroxidase	ssDNA	Single layer	0.16 M	0.16 M	60 min	[52]
	Subtilisin	Gelatin	Bloch surface wave	0.01 mg mL^{-1}	1.8 pM	20 min	[152]
Antibody	Sheep IgG	Protein A	Single layer	10-500 μg mL^{-1}	0.6 μg mL^{-1}	90 min	[48]
	Human IgG	Anti-human IgG	Single layer	0.2-100 μg mL^{-1}	0.2 μg mL^{-1}	20 min	[49]
	Human IgG	Human anti-IgG antibody	Waveguide	6.7×10^{-10}- 6.7×10^{-6} M	2.3×10^{5} nm M^{-1} (1.5 fg)	Overnight	[34]
	Rabbit IgG	Anti-rabbit IgG	Microcavity	0.07-3 mg mL^{-1}	70 μg mL^{-1}	60 min	[50]
Whole cell	Bacteria (*L. acidophilus*)	Aptamer Hemag1P	Single layer	10^{6}-10^{7} cells mL^{-1}	10^{6} cells mL^{-1}	20 min	[53]
	Bacteria (*E. coli*)	*E. coli* antibody	Single layer	10^{3}-10^{7} cfu mL^{-1}	10^{3} cfu mL^{-1}	150 min	[155]
	Bacteria (*E. coli*)	Peptide	Single layer	10^{3}-10^{5} cells mL^{-1}	10^{3} cells mL^{-1}	60 min	[20]
	HeLa cells	Antibody	Rugate filter particles	1.5×10^{5}-2×10^{5} cells mL^{-1}	1.5×10^{5} cells mL^{-1}	around 5 h	[91]
	Bacteria	Vancomycin	Microcavity	100-1000 cells mL^{-1}	20 cells mL^{-1}	n/d	[55]

	Yeast cells and its components	Antibody	Single layer	5-20 μg L^{-1} (fibre optic sensor), 100-1000 μg L^{-1} (photo-luminescence sensor)	5-20 μg L^{-1} (fibre optic sensor), 100 μg L^{-1} (photo-lumine-scence sensor)	60 min	[54]
Virus	M13KO7 bacteriophage	APTES and glutaraldehyde	Bloch surface wave	32 μg mL^{-1}	32 μg mL^{-1}	20 min	[57]
	Bacteriophage MS2	Rabbit anti-MS2 antibody	Single layer	1×10^{6}-1×10^{12} pfu mL^{-1}	2×10^{7} pfu mL^{-1}	45 min	[56]
Protein	Bovine serum albumin	Oxidized PSi surface	Single layer	150 pM-15 μM	20 pM	60 min	[59]
	Streptavidin	Biotin	Microcavity	0.5-5 μM	0.5 μM	20 min	[156]
	Lectin and Norovirus (NV)-like particles	Glycan	Ring resonator	500 nM (lectin),0.25-20 μg mL^{-1} (NV particles)	500 nM (lectin), 250 ng mL^{-1} (NV particles)	20 min	[60]
Other small analyte	Glucose, urea, and heavy metals	Glucose oxidase and urease	Single layer	0.5-3 mM (Glucose and urea) 10 nM^{-1} mM (Heavy metal)	0.5 mM (Glucose and urea);10 nM (Heavy metal)	5 min	[157]
	Trypsin inhibitor	Trypsin	Double layer	10-200 ng mL^{-1}	10 ng mL^{-1}	Few min	[159]
	Opiate	Opiate-analogue (M3G)	Bragg reflector	1-10,000 ng mL^{-1}	300 ng mL^{-1}	60 min	[61]
	Opiate	Opiate-analogue (M3G)	Bragg reflector	0.018-10.8 μM	0.018 μM	60 min	[62]
	Vancomycin	Peptide	Double layer	0.005-0.1 mg mL^{-1}	0.005 mg mL^{-1}	around 20 min	[158]

7. OPTICAL BIOSENSING ON PSi

Optical biosensing on PSi has been carried out for the detection of wide range of biomolecules including short DNA oligonucleotides, enzymes, antibody, whole cells (bacteria and yeast), viruses, and other small and large molecules by immobilizing its corresponding capture probe on PSi surface (Table 1). When a target analyte binds with capture probe on the PSi optical biosensor, the water (or air) present in porous structure is replaced with target analytes resulting in a change in the average refractive index of the PSi layer. This refractive index change can be detected as a shift in the wavelength of the characteristic optical spectral peak. In case of several PSi enzyme biosensors, substrate for corresponding enzyme is filled in the porous structure, which degrades if enzyme is present in sample and the average refractive index of the film decreases. The optical transduction event of binding of target biomolecules in PSi optical biosensor is monitored by measuring the reflectance, photoluminescence, absorption, or transmittance.

7.1. DNA Detection

DNA biosensor has immobilized complementary DNA on its surface as a capture probe, which binds to the target DNA from the sample due to the DNA-DNA hybridization. PSi optical biosensor has been prepared by fabricating different optical structures such as single layer, Bragg reflector, waveguide, Bloch surface wave, and ring resonator for detection of DNA. A pioneering work of Sailor and colleagues in 1997 on PSi optical biosensor led to the momentous interest on PSi for optical biosensing applications [13]. They demonstrated the applicability of PSi in optical biosensing by fabricating single layer interferometer for the detection of wide range of molecules including DNA, proteins (streptavidin and antibodies), and small organic molecules (biotin and digoxigenin) at pico and femtomolar analyte concentrations. PSi single layer surface was oxidized and silanized before attachment of these biomolecules.

Recently, PSi ring resonator structure was demonstrated for selective and sensitive detection of DNA [43]. The ring resonator structure was patterned on PSi slab waveguide and then functionalized with APTES and succinimidyl 3-(2-pyridyldithio)propionate linker molecule for the immobilization of thiol-modified 16mer probe DNA. A specific detection of target complementary DNA was observed with surface sensitivity of 4 pm nM^{-1} and a limit of detection of 3 nM. PSi grating-coupled Bloch surface wave and Bloch sub-surface wave propagating mode optical biosensor has been demonstrated for the detection of DNA and small molecules [94]. PSi Bloch surface wave is confined at the multilayer-air interface, which can be helpful to detect larger molecules with high sensitivity whereas PSi Bloch sub-surface wave is confined just beneath the surface and has a strong sensitivity to small molecules that penetrate the porous matrix. The detection of two small molecules of 3-APTES and Sulfosuccinimidyl-4-(N-maleimidomethyl) cyclohexane-1-carboxylate (Sulfo-SMCC), which also acts as linker molecules and one large molecule of 40 base DNA oligonucleotide was carried out. A large resonance shifts (>1°) was observed for 3-APTES and Sulfo-SMCC molecules for all three Bloch surface wave, Bloch sub-surface, and waveguide resonant modes indicating that small molecules readily penetrated the porous matrix. Among all three modes, a novel Bloch sub-surface mode showed largest response to small molecule detection with 33% enhancement in comparison to the benchmarked waveguide sensor. In case of large DNA molecule, Bloch surface wave mode showed largest resonance shift (~0.29°) demonstrating 6-fold improvement in detecting large molecules when compared to Bloch sub-surface and waveguide modes.

A highly sensitive and specific PSi biosensor for detection of DNA with a limit of detection of 1 nM is also reported in a recent study [149]. Electrokinetic method called isotachophoresis (ITP) was implemented in a microfluidic platform to focus the target DNA within a moving ITP plug and was accurately delivered it to the PSi biosensor. PSi optical biosensor showed detection of DNA in the range of 1×10^{-9} and 10×10^{-9} M with 1000 fold improvement in a limit of detection in comparison to standard assay. A label-free detection of DNA has been done using PSi resonant waveguide biosensor [45]. PSi waveguide structure was prepared by applying different current densities to form low porosity layer on the top of high porosity layer. A probe DNA was linked to the oxidized PSi waveguide by using 3-APTES and glutaraldehyde chemistry. The binding of complementary DNA to probe DNA was detected by measurement of a shift of the waveguide resonance angle. The waveguide biosensor showed DNA concentration dependent resonance shift and no shift in case of non-complementary DNA suggesting very high specificity of sensor. In addition to high specificity, low detection limit of 50 nM (5 pg mm^{-2}) DNA was calculated.

7.2. Enzyme Detection

Enzymes are ideal biomarkers for a range of diseases including cancer, cardiovascular, neurodegeneration, and chronic wounds. Also, an activity of enzymes gives the idea of normal or abnormal cellular function, which is useful in detection of infections. Another important characteristic of enzyme is that it reacts with corresponding substrate under specific reaction conditions, for example, pH, temperature, and ionic strength. The detection of enzyme on biosensor can be done by immobilizing substrate for the enzyme and determining either the rate of product formation or substrate depletion during enzyme catalyzed reaction on sensor.

PSi microcavity based optical biosensor was prepared for multiplexed enzyme detection from wound fluids [150]. *Staphylococcus aureus* (*S. aureus*) is most commonly found pathogen in infected chronic wounds, which delays wound healing process. Therefore, biomarker selected was bacterial enzyme sortase A, which is found in the cell membrane protein of *S. aureus*. PSi microcavity structure was stabilized by thermal hydrosilylation of undecylenic acid and sortase A fluorogenic peptide substrate was then immobilized using EDC/NHS. A measured fluorescence intensity increased linearly with increasing concentration of sortase A enzyme from 4.6×10^{-12} M to 4.6×10^{-8} M with a limit of detection of 8×10^{-14} M. Furthermore, an array of peptide spots specific for matrix metalloproteinases (MMP) and sortase A was produced on a PSi surface via robotic printing of two different fluorogenic peptide substrates to demonstrate multiplexed detection on biosensor. PSi microcavity surface incubated with wound fluid showed only blue fluorescence emitted from the rows of MMP peptide substrate spots due to the cleavage of peptide substrate by MMP. This also confirmed the presence of MMP and absence of sortase A in wound fluid sample. When PSi microcavity surface incubated with bacterial culture medium, it showed green fluorescence emitted from the rows containing sortase A peptide substrate spots. Thus it was confirmed that sortase A present in bacterial culture medium sample did not cleave the MMP peptide substrate. In an another study, sensitive, selective, and real-time detection of MMPs found in the wound exudates was demonstrated using fluorescence based PSi resonant microcavity biosensor [151]. The fluorogenic MMP peptide substrate was immobilized on the hydrosilylated surface via EDC and NHS surface chemistry. In the presence of MMPs, peptide substrate on PSi sensor was fragmented and the fluorescence at 446.5 nm was observed. The fluorescence intensity of fluorophore embedded in PSi matrix was higher than the fluorescence intensity of fluorophore in the buffer solution at the same MMP concentration owing to the fluorescence enhancement by photonic structure of PSi microcavity. Furthermore, fluorescence enhancement effect of PSi resulted into high sensitivity with limit of detection of 7.5×10^{-19} M and it also allowed the measurement of MMPs in human wound fluid.

PSi Bloch surface wave biosensor was developed for the detection of protease [36,152]. PSi sensor was fabricated based on a periodic multilayered Bragg reflector mounted on a glass substrate, which supports optical Bloch surface modes. Surface of PSi was chemically modified by thermal hydrosilylation in undecylenic acid followed by reaction with 1-amino-hexa(ethylene glycol) to form a layer that resists non-specific adsorption of proteins on the surface. Then, a gelatin, which is a substrate for the protease was covalently attached on surface. The protease enzyme subtilisin activity caused the degradation of gelatin in the PSi and resulted in a spectral blue shift of the surface wave mode [152]. A magnitude of resonance shift was directly proportional to the concentration of subtilisin and digestion time with a low detection limit of 370 pM. In addition, band edge was remained at the same position in the reflectivity spectrum in both control and enzyme experiments indicating that bulk photonic structure was insensitive to the proteolytic reaction and its degradation products and therefore can be used as an internal reference to exclude any nonspecific adsorption and bonding that may occur through the bulk of the film [36].

The detection of human α-thrombin by PSi aptasensor using aptamer as a capture probe is reported recently [153]. Human α-thrombin also known as coagulation factor II is a serine protease, which has a very vital role in coagulation and hemostasis in the body by converting soluble fibrinogen into insoluble fibrin. Detection of Human α-thrombin is very important because high level of enzyme in the blood induces pathological coagulation disorders and also serious damages to human health. To prepare aptasensor, PSi single layer was thermally oxidized and amino silanized using APTES. Then, 17-mer thrombin binding aptamer analogue was synthesized *in situ* on a PSi surface by automated DNA synthesizer. The prepared PSi aptasensor showed very high selectivity and reversibility for thrombin with affinity constant of 14±8 nM and limit of detection of 1.5±0.3 nM as measured

from the spectroscopic reflectometry, and quantified by fast Fourier transform analysis.

The intracellular enzyme L-lactate dehydrogenase (LDH) is present in most of the tissues of human and is one of the most common physical markers in the disease diagnosis. It is released from the damaged cells, and therefore an increased level of this enzyme is observed in the blood when there is a cell death due to the injury or disease. Additionally, high levels of LDH have been associated with pulmonary cancer, leukemia, melanoma, and chronic wounds. Therefore, luminescence-enhancing PSi microcavity biosensor was prepared for the detection of LDH [127]. The fluorescence enhancement effects inside PSi microcavity biosensor was carried out by immobilizing non-fluorescent resazurin dye on the PSi surface via thermal hydrocarbonization, thermal hydrosilylation, and acylation, which converts into strongly fluorescent product resorufin by enzymatic reduction. Thermally hydrocarbonized PSi modified with hydrosilylation showed an excellent surface stability than the PSi treated with thermal hydrosilylation only. This was due to hydrocarbon layer formed on the thermally hydrocarbonized PSi samples that prevented the surface from being oxidized in resazurin aqueous solutions. The fluorescence signal obtained from biosensor upon detection of LDH was 10 and 5 fold higher than that on single layer and detuned microcavity, respectively. The biosensor displayed excellent limit of detection of 0.08 U mL^{-1}, and detection range between 0.16 and 6.5 U mL^{-1}, which is concentration range of LDH in normal as well as damaged tissues. Moreover, PSi microcavity showed very high selectivity for LDH with 30% less reagent usage and three fold decrease in analysis time than the standard LDH test [127].

Enzyme activity is also studied in real-time using PSi double layer biosensor [41]. PSi double layer with large pores of around 100 nm in diameter on the top layer and small pores of around 6 nm in lower layer was fabricated by varying the current density so that enzyme trapping and catalysis reaction takes place in top layer whereas reaction products of catalysis can only enter into the bottom layer. Thermally oxidized PSi double layer was then immobilized using pepsin by electrostatic adsorption. When the substrate α-casein was introduced to PSi biosensor, initially a value of the optical thickness ($2nL$) of top layer was increased due to the protein accumulation. Then, pepsin starts digesting the casein and digestion products enter into the lower layer and escape into a solution due to which a value of $2nL$ was decreased for top layer and increased for bottom layer as measured from Fourier transforms of reflectivity spectra. Also, no change in $2nL$ value of bottom layer was observed in the presence of competitive inhibitor (pepstatin A) or in the absence of pepsin. This PSi double layer interferometer allowed the quantification of enzyme kinetics in a real-time by within a volume of $5nL$.

A detailed study on the effect of different stabilization and functionalization methods on PSi microcavity structure for the preparation of biosensor to detect glucose oxidase has been carried out [84]. Two different PSi surface modification methods were used where one method consisting of initial thermal oxidation of PSi microcavity surface followed by reaction with APTES molecules while second method involved direct surface modification of as-etched PSi surface by APTES. The glucose oxidase was immobilized on the PSi via APTES and glutaraldehyde linker molecules. A direct silanization reaction of microcavity produced only slight change in the Q factor whereas initial thermal oxidation reduced the Q factor to half of its initial value. Microcavity biosensor displayed a detection limit of 25 nM and a linear increase in the resonance shift with glucose oxidase concentration in the range of 0.1-14 μM. The detection of urease enzyme is also reported using single layer PSi optical biosensor [58]. Photoluminescence of PSi was changed after the immobilization of urease and reaction with substrate urea. The immobilized urease enzyme exhibited linear response against urea concentrations in the range of 3.3×10^{-5}- 2.4×10^{-4} M with reusability of five times and a shelf life of 15 days.

7.3. Antibody detection

PSi optical biosensor can be made with antigen as capture molecule for the highly selective detection of antibody in target sample. An optical interference immunosensor based on TiO_2-coated PSi film was demonstrated for the detection of immunoglobulin G (IgG) [48]. In order to increase the chemical stability of PSi surface, TiO_2 sol-gel precursor was deposited on the oxidized (by ozone gas) PSi sample by spin coating followed by heating in a tube furnace at 500 °C in air. TiO_2 coated PSi showed greater stability in buffer solutions within pH range of 2-12 in comparison to thermally oxidized PSi (at 700 °C in air), which dissolved in solutions at pH>7. The stability study of TiO_2-coated PSi film was further followed with an immunosensor application. PSi with physically adsorbed protein A showed specific binding to the rabbit anti-sheep IgG and then to the secondary antibody of sheep IgG. Furthermore, protein

A did not bind with chicken IgG in control experiments due to the lack of affinity, which also confirmed the specificity of protein A modified immunosensor to the rabbit anti-sheep IgG. A linear detection of sheep IgG was observed in the range from 10-500 μg mL^{-1} with a limit of detection of 0.6 μg mL^{-1}.

A novel transducer mechanism based on the change in PSi structural colour due to the biomolecular binding events was proposed for detection of antibody [49]. PSi with oxidized surface was used for immobilization of anti-human IgG through silane linker. A target antibody human IgG was detected by interaction with antibody immobilized PSi followed by incubation with horseradish peroxidase (HRP)-conjugated antibody (specific for human IgG) and tetramethylbenzidine (TMB). An optical detection signal was amplified on a PSi film due to the HRP enzyme catalyzed reaction of TMB substrate and was observed as sharp increase in EOT of PSi layer. This amplification of PSi signal was caused by an intermediate radical cation produced during the enzyme catalyzed oxidation of TMB. A very high detection sensitivity of human IgG down to a concentration of 0.2 μg mL^{-1} was possible by this transducer mechanism.

A label-free PSi optical biosensor was developed for the highly repeatable and specific detection of IgG in serum and whole blood samples [47]. Pore size of PSi microcavity structure was optimized with inherent filtering capabilities to exclude cells and other large proteins from interacting with the transducer surface. Fabricated PSi microcavity was thermally oxidized and then silanized using 3-aminopropyltrimethoxysilane. An amine terminated PSi surface was subsequently functionalized with biotin-streptavidin chemistry to immobilize anti-rabbit IgG. PSi microcavity biosensor showed high target binding specificity, minimal cross reactivity, and a linear detection range for rabbit IgG between the values of 2-10 mg mL^{-1}.

PSi double layer immunosensor has been also fabricated by varying the current density to prepare higher porosity (large pores) top layer and lower porosity (small pores) bottom layer [154]. PSi was thermally oxidized at 600 °C and capture probe protein A was then adsorbed on the top layer. The rabbit IgG was captured on the top layer through protein A and resulted in shifts in the fast Fourier transform peak corresponding to the top layer. Interferents such as sucrose or buffer solutions could enter the both layers, which was corrected for zero-line drift by eliminating from the optical signals. PSi immunosensor showed 10 times greater response to IgG than the change observed for strongly adsorbed protein A. Equilibrium dissociation constant K_D of 3×10^{-7} mol L^{-1} was observed for rabbit IgG/protein A.

7.4. Cell detection

Whole cell detection of bacteria, yeast, and other microorganisms plays an important role in the food and water safety studies. Also, cell detection on optical biosensor using antibody modified PSi allows their detection and quantification. Recently, a new sensing strategy for rapid detection of bacteria based on its blockage effect on PSi nanopore array has been reported [155]. The *Escherichia coli* (*E. coli*) bacteria were selectively and rapidly captured on the nanopore array resulting in pore blockages, which was measured by using indirect Fourier transformed reflectometric interference spectroscopy. In a direct FT-RIS method, EOT shift is directly proportional to analyte concentration and it changes when the analyte captured inside the pore channel. However, large bacteria, virus and cells, which are of micrometer scale cannot enter the porous matrix due to the small diameter of pores. Therefore, for the detection of large bioanalytes, indirect FT-RIS method based on pore blockage was used. EOT shift was decreased linearly with an increase of bacterial density within a range of 10^3 to 10^7 cfu mL^{-1} due to the pore blockage. The selectivity of immobilized antibody to the *E. coli* was further confirmed by using non-target bacteria, *Nox* and *P17*, which did not show any change in EOT shift due to the no interaction with antibody. This sensing strategy approach is particularly advantageous for the rapid and label-free detection of bacteria and other cells where the target analyte infiltration into the nanopores is not required.

A direct detection of probiotic bacteria *Lactobacillus acidophilus* (*L. acidophilus*) has been carried out by preparing aptamer based PSi biosensor [53]. PSi thin film was prepared with an anodization process of a silicon wafer at a current density of 300 mA cm^{-2} for duration of 30 s and thermally oxidized in order to prepare hydrophilic scaffold. After surface stabilization, PSi biofunctionalization was carried out in a three-step to immobilize aptamers on oxidized surface. In a first step, oxidized surface was silanized with (3-mercaptopropyl) trimethoxysilane in order to obtain a thiolated surface. Then, thiolated surface was reacted with the acrydite modified aptamers to form thioether bonds. In a third and final step, maleimide was used to block the residual thiol groups to minimize the subsequent non-spe-

cific reaction with buffers or sample components. The *L. acidophilus* cells were not able to penetrate into the porous nanostructure due to their larger size and therefore captured on a surface of porous nanostructure by the immobilized aptamer Hemag1P. By using PSi nanostructure 10^7 cells mL^{-1} of bacteria were detected. However, to increase the dynamic range of biosensor, further tuning of the nanostructure of a PSi was carried out by reducing the pore diameter to exhibit mesoporous morphology with improved optical properties. After the tuning of porous structure, low concentration of bacteria of 10^6 cells mL^{-1} was detected with distinguishing between live and dead cells and high selectivity and specificity.

The detection of yeast cells and its components which were discharged in the air inside and in the vicinity of a biotechnology plant producing amino acids has been carried out using PSi optical immune sensors [54]. Photoluminescence and fibre optic in combination with the chemical luminescence of PSi were measured after the polyclonal antibody immobilized on PSi surface. It was observed that the fibre optic sensor was more sensitive (5-20 $\mu g\ L^{-1}$) than the photoluminescence sensor (100 $\mu g\ L^{-1}$) and also its sensitivity was comparable to the enzyme-linked immunosorbent assay.

7.5. Virus detection

PSi biosensor has been developed for detection of viruses by immobilizing an antibody against it on a surface. PSi Bloch surface wave and sub-surface wave composite biosensor has been designed for the detection of M13KO7 bacteriophage, latex nanospheres, and small linker molecules including APTES and glutaraldehyde [57]. The bacteriophage was attached to PSi surface through APTES and glutaraldehyde linker molecules. APTES and glutaraldehyde penetrated the porous matrix due to their small size with resonance shifts for Bloch surface wave and first Bloch sub-surface wave mode (in gradient index profile) were 1.6°; 2.18° and 1.97°; 2.66°, respectively. While bacteriophage did not infiltrate the porous matrix due to its large size and therefore resonance shift only in Bloch surface wave mode with 0.31° was observed [57]. The detection of virus bacteriophage MS2 was carried out using PSi single layer biosensor [56]. Two different methods consisting of carbodiimide and aryldiazirine cross-linker were employed for attachment of rabbit anti-MS2 antibody on the PSi surface. The carbodiimide functionalized PSi displayed good pore penetration and binding efficiency for the probe antibody due to the hydrophilic surface whereas diazirine functionalized PSi showed comparatively less binding efficiency owing to the pronounced hydrophobic surface. PSi biosensor allowed the selective detection of bacteriophage MS2 by measuring the fluorescence within a viral concentration range of 1×10^6 to 1×10^{12} plaque-forming units (pfu) mL^{-1} and a limit of detection of 2×10^7 pfu mL^{-1} [56].

7.6. Protein detection

Recently, Mariani et al. [59] has prepared ultrasensitive biosensor based on the nanostructured PSi interferometer for the femtomole detection of proteins. They proposed a new sensitive and robust signal processing strategy based on the calculation of average value of spectral interferograms over wavelength called IAW, by subtraction of reflectance spectra acquired after adsorption of protein (bovine serum albumin, BSA) inside the porous matrix from a reference spectrum recorded in acetate buffer. BSA concentrations ranging from 150 pM to 15 μM were detected in a PSi interferometer by using IAW signal processing strategy. In addition, good signal to noise ratio and reproducibility with detection limit of 20 pM was estimated, which is a lowest detection limit that has been reported using PSi interferometer.

Zhao et al. [156] has developed open-ended PSi microcavity membranes for a real-time flow-through biosensing of streptavidin. A close-ended nanoporous sensor has drawbacks of inefficient analyte transport and slow responses for detecting large molecules including proteins and nucleic acids in dilute solutions due to their slow diffusion rates. Therefore, open-ended PSi nanoporous membranes were used in a flow-through mode, allowing analyte solutions to pass through the nanopores resulting in improved molecule transport efficiency and reduced sensor response time. A 6-fold improvement in sensor response time was observed in case of flow-through PSi membrane than the flow-over PSi mode when the streptavidin was attached to biotin-functionalized PSi. Furthermore, in comparison to the close-ended on substrate PSi sensor, the open-ended flow-through PSi membrane showed larger resonance wavelength shifts for different concentrations (0.5-5 μM) of streptavidin [156].

7.7. Small analyte detection

The detection of glucose, urea, and heavy metals has been carried out using PSi optical biosensor [157]. A change in photoluminescence of PSi was

observed with respect to the variations in medium pH due to enzyme-substrate reaction. The enzymes glucose oxidase and urease were used as a bioselective material for PSi biosensor. Glucose oxidase catalyzes the conversion of glucose to gluconic acid and shifts the pH of a medium to acidic whereas urease converts the urea into ammonia with shifting medium pH to alkaline. By increasing glucose and urea concentration from 0 to 3.0 mM in the respective glucose oxidase and urease containing medium, photoluminescence intensity of PSi biosensor was increased by 1.7 and 1.45 times, respectively. On the contrary, photoluminescence quantum yield of PSi was restored in the presence of heavy metal ions (Cu^{2+}, Pb^{2+}, and Cd^{2+}) in the tested solution owing to an inhibition of the glucose oxidase and urease enzyme catalyzed reactions.

Pacholski et al. [158] has fabricated PSi double layer biosensor for the detection of small molecule vancomycin using reflective interferometric Fourier transform spectroscopy (RIFTS) method. In PSi double layer sensor, top layer works as a sensing channel and bottom layer acts as a reference channel. A capture probe peptide was covalently immobilized on the thermally oxidized PSi surface through coupling reaction using EDC/NHS. A double layer sensor showed a shift in FFT peak to larger values and an increase in the intensity of FFT peak due to the binding of vancomycin on peptide modified sensor. Furthermore, PSi double layer displayed both qualitative specific detection of vancomycin and quantitative information about binding events, for example, equilibrium binding constants. PSi biosensor is also developed for detection of target compounds for drug screening and discovery. PSi double layer interferometer was fabricated for the post-column detection of trypsin inhibitor from complex samples by immobilizing trypsin as a capture probe using RIFTS method [159]. PSi double layer was functionalized with trypsin by standard amino-silane and glutaraldehyde chemistry in the upper layer. The detection of trypsin inhibitor was measured as a change in the EOT when bound to the trypsin on PSi. A linear relationship was observed between the optical signals and concentration of trypsin inhibitor in a range of 10-200 ng mL^{-1}.

7.8. *In Vivo* and *In Vitro* PSi biosensor

For *in vivo* implantable applications, biosensor should be hydrolytic stable under physiological conditions, biocompatible and should allow the measurement of an optical signal through the tissue. Tong et al. [37] has demonstrated for the first time that thermally hydrocarbonized PSi rugate filters are both biocompatible and optically functional for lab-on-a-chip and subcutaneous biosensing applications. PSi rugate filters with different surface chemistries including thermally oxidized (at temperatures of 500 °C, 600 °C, and 800 °C) and thermally hydrocarbonized were prepared. Thermally hydrocarbonized PSi showed good stability and optical properties over the entire timeframe of the experiment for 14 days. Whereas thermally oxidized PSi at 500 °C, 600 °C, and 800 °C dissolved over 4, 6, and 8 days, respectively, and also lost its optical properties. *In vitro* biocompatibility study of these surfaces showed cytotoxicity from thermally hydrocarbonized and certain thermally oxidized PSi. However, cytotoxicity of thermally hydrocarbonized PSi was fully eliminated by pre-incubation in Dulbecco's modified eagle medium for 10 days at 37 °C. Furthermore, thermally hydrocarbonized PSi surface did not hinder the proliferation of fibroblasts. *In vivo* biocompatibility of PSi surface was further studied in a mouse model. When thermally hydrocarbonized PSi rugate filters were surgically implanted subcutaneously with implant material polycaprolactone as a control, no swelling, low inflammatory response, and structured with good tissue growth onto the implant surface was observed indicating good biocompatibility of PSi structure *in vivo*. The toxicity effect of degradation product of this material namely silicon and boron species on liver and spleen showed neither tissue necrosis nor obvious inflammatory cell infiltration. In addition, optical properties of PSi biosensor were maintained *in vivo* as recorded through the skin.

In vitro real-time monitoring of living cells has been performed by the concept of "smart Petri dish" using PSi photonic crystal [42]. PSi rugate filter was fabricated and coated with polystyrene via undecylenic acid terminated surface. The hepatocytes were seeded on polystyrene filled PSi rugate filter and physiological changes in hepatocytes were monitored by measuring the intensity of light scattered from a PSi surface using charge-coupled device spectrometer. When the incident light source was positioned off the surface normal, the cells present on the PSi photonic crystal surface generated diffuse scattering and some of the light incident was measured by spectrometer. It was reported that scattered light intensity was increased due to morphological changes when cells were exposed to the toxins cadmium chloride or acetaminophen. Furthermore, PSi photonic crystal sensor allowed the detection of cell viability in non-invasive, real-time and faster manner than the other conventional

techniques for *in vitro* monitoring of cell morphology.

7.9. PSi photonic particles as biosensor

PSi photonic particles also called "smart dust" have been developed for the detection of enzyme [90], volatile organic compounds [160], and single cell biosensing [91,161]. PSi photonic particles display similar advantages like films, for example, particles can be easily chemically modified to increase stability in a physiological media and can be functionalized with different bio-recognition molecules to give them selectivity for target biomolecules [161]. Recently, Guan et al. [91] has prepared antibody functionalized PSi microparticles for the selective detection of HeLa cells. PSi rugate filter with a high reflectance band in the reflectivity spectrum was fabricated and surface was modified via the Cu(I)-catalyzed alkyne-azide cyclo addition reaction and succimidyl activation. The microparticles of PSi prepared by ultrasonic fracture were then immobilized with antibody by covalent attachment. PSi photonic particles showed highly specific and selective capture of HeLa cells presenting receptors or fluorescent proteins via antibody-antigen interaction without any cross reactivity. Furthermore, optical reflectance property of microparticles was intact after the particle preparation and even after binding with cells, which allowed the biosensing in a real-time.

Gupta et al. [90] has reported a label-free specific detection of enzyme MMP at low concentrations using PSi photonic microsensors. PSi rugate filter structure was modified with hydrosilylation of an alkyne to form a stable Si-C bond and poly(ethylene glycol) to avoid non-specific adsorption of proteins. The peptide specific for an enzyme MMP was immobilized through EDC/NHS chemistry and then coupled with another polymer layer. PSi photonic microsensor displayed concentration dependent shift in a wavelength of main peak in reflectivity spectrum due to the cleavage of peptide sequence by MMP. The detection range of 1 nM to 1.5 μM with as low as 1 nM concentration of MMP enzyme was determined using microsensor. Furthermore, picogram amount of detection was demonstrated for enzyme released from epithelial cells. PSi photonic microparticles based on distributed Bragg reflector was studied for detection of volatile organic compounds including methanol and hexane. An increase in refractive indices of entire particle and in turn red shift in the photonic peak was observed when the vapors condensed in a porous matrix of photonic particle [160].

8. CONCLUSION AND FUTURE PROSPECTS

In summary, this review highlights recent developments in PSi optical biosensor. PSi optical biosensors are studied enormously than the other sensing platforms due to its important optical and physical properties. The fabrication of different PSi optical biosensor and its effect on the performance of biosensor, for example, sensitivity, selectivity, and response time have been highlighted. A low-cost, label-free, real-time monitoring, highly sensitive, and selective biosensors are currently of need for lab-on-a-chip and point of care diagnostics. PSi optical biosensor has demonstrated all these properties for detection of wide range of biomolecules including large protein, enzyme, antibody, DNA, virus, whole cell, and small analytes. PSi optical structures are also developed for the *in vitro* real-time monitoring of living cells. Furthermore, good biocompatibility, stability, and optical properties of PSi have opened the door for development of implantable biosensor for *in vivo* optical biosensing applications. However, there are several challenges associated with PSi optical biosensor which needs to be addressed for commercialization of the device. First major challenge is the detection of target analytes at a very low concentration from complex biological media such as whole blood for early diagnosis of diseases. The early detection of biomarkers can be highly advantageous in controlling the development of disease, for example, cancer. Secondly, the stability of PSi optical biosensor for *in vivo* implantable applications needs to be further addressed using different surface modification strategies. In future, more number of studies will be focused on integration of PSi optical biosensors with microfluidic systems for highly sensitive and rapid detections. Furthermore, multiplexed detection of different biomolecules on a microarray of PSi for parallel biosensing will be on a center of future studies to further develop as a point of care device.

REFERENCES

[1] A.D. McNaught and A. Wilkinson, *IUPAC. Compendium of Chemical Terminology, Gold Book* (Oxford: Blackwell Scientific Publications, 1997).

[2] D.R. Thevenot, K. Toth, R.A. Durst and G.S. Wilson // *Pure Appl. Chem*. **71** (1999) 2333.

[3] D.R. Thevenot, K. Toth, R.A. Durst and G.S. Wilson // *Biosens. Bioelectron*. **16** (2001) 121.
[4] A. Jane, R. Dronov, A. Hodges and N.H. Voelcker // *Trends Biotechnol.* **27** (2009) 230.
[5] L.T. Canham // *Appl. Phys. Lett.* **57** (1990) 1046.
[6] A. Uhlir // *Bell Syst. Tech. J.* **35** (1956) 333.
[7] L.T. Canham // *Adv. Mater.* **7** (1995) 1033.
[8] L.T. Canham, J.P. Newey, C.L. Reeves, M.R. Houlton, A. Loni, A.J. Simons, T.I. Cox // *Adv. Mater.* **8** (1996) 847.
[9] L.T. Canham, C.L. Reeves, J.P. Newey, M.R. Houlton, T.I. Cox, J.M. Buriak and M.P. Stewart // *Adv. Mater.* **11** (1999) 1505.
[10] P.N. Patel, V. Mishra, A.K. Panchal and N.H. Maniya // *Sensors & Transducers* **139** (2012) 79.
[11] S. Chan, P.M. Fauchet, Y. Li, L.J. Rothberg and B.L. Miller // *Phys. Status Solidi A* **182** (2000) 541.
[12] A. Foucaran, F. Pascal-Delannoy, A. Giani, A. Sackda, P. Combette and A. Boyer // *Thin Solid Films* **297** (1997) 317.
[13] V.S.-Y. Lin, K. Motesharei, K.-P.S. Dancil, M.J. Sailor and M.R. Ghadiri // *Science* **27**8 (1997) 840.
[14] P.N. Patel, V. Mishra, A.K. Panchal and N.H. Maniya // *J. International Academy of Physical Sciences* **16** (2012) 275.
[15] F.A. Harraz // *Sens. Actuators B: Chem*. **202** (2014) 897.
[16] C. RoyChaudhuri // *Sens. Actuators B: Chem*. **210** (2015) 310.
[17] Y. Lee and K. Lee // *Sens. Actuators B: Chem.* **202** (2014) 417.
[18] S.-H. Park, D. Seo, Y.-Y. Kim and K.-W. Lee // *Sens. Actuators B: Chem*. **147** (2010) 775.
[19] A.A. Ensafi, N. Ahmadi and B. Rezaei // *Sens. Actuators B: Chem*. **239** (2017) 807.
[20] E. Tenenbaum and E. Segal // *Analyst* **140** (2015) 7726.
[21] L. Gu, D.J. Hall, Z. Qin, E. Anglin, J. Joo, D.J. Mooney, S.B. Howell and M.J. Sailor // *Nat. Commun*. **4** (2013).
[22] E. Tasciotti, X. Liu, R. Bhavane, K. Plant, A.D. Leonard, B.K. Price, M.M. Cheng, P. Decuzzi, J.M. Tour, F. Robertson and M. Ferrari // *Nat. Nanotechnol.* **3** (2008) 151.
[23] F. Cunin, T.A. Schmedake, J.R. Link, Y.Y. Li, J. Koh, S.N. Bhatia and M.J. Sailor // *Nat. Mater*. **1** (2002) 39.
[24] M.A. Whitehead, D. Fan, P. Mukherjee, G.R. Akkaraju, L.T. Canham and J.L. Coffer // *Tissue Eng. Part A* **14** (2008) 195.
[25] N.H. Maniya, S.R. Patel and Z.V.P. Murthy // *Chem. Eng. Res. Des.* **104** (2015) 551.
[26] N.H. Maniya, S.R. Patel and Z.V.P. Murthy // *Appl. Surf. Sci*. **330** (2015) 358.
[27] J. Salonen, L. Laitinen, A.M. Kaukonen, J. Tuura, M. Bjorkqvist, T. Heikkila, K. Vaha-Heikkila, J. Hirvonen and V.P. Lehto // *J. Control. Release* **108** (2005) 362.
[28] J. Salonen, A.M. Kaukonen, J. Hirvonen and V.P. Lehto // *J. Pharm. Sci.* **97** (2008) 632.
[29] X.G. Zhang // *J. Electrochem. Soc.* **151** (2004) C69.
[30] J.M. Buriak // *Chem. Rev*. **102** (2002) 1271.
[31] K.-P.S. Dancil, D.P. Greiner and M.J. Sailor // *J. Am. Chem. Soc.* **121** (1999) 7925.
[32] C. Pacholski, M. Sartor, M.J. Sailor, F. Cunin and G.M. Miskelly // *J. Am. Chem. Soc.* **127** (2005) 11636.
[33] N.H. Maniya, S.R. Patel and Z.V.P. Murthy // *Optik* **125** (2014) 828.
[34] S. Pal, E. Guillermain, R. Sriram, B.L. Miller and P.M. Fauchet // *Biosens. Bioelectron.* **26** (2011) 4024.
[35] S. Li, D. Hu, J. Huang and L. Cai // *Nanoscale Res. Lett.* **7** (2012) 79.
[36] H. Qiao, A.H. Soeriyadi, B. Guan, P.J. Reece and J.J. Gooding // *Sens. Actuators B: Chem.* **211** (2015) 469.
[37] W.Y. Tong, M.J. Sweetman, E.R. Marzouk, C. Fraser, T. Kuchel and N.H. Voelcker // *Biomaterials* **74** (2016) 217.
[38] N.H. Maniya, S.R. Patel and Z.V.P. Murthy // *Superlattice. Microst.* **85** (2015) 34.
[39] L. Cheng, E. Anglin, F. Cunin, D. Kim, M.J. Sailor, I. Falkenstein, A. Tammewar and W.R. Freeman // *Br. J. Ophthalmol*. **92** (2008) 705.
[40] L.T. Canham // *Nanotechnology* **18** (2007) 185704.
[41] M.M. Orosco, C. Pacholski and M.J. Sailor // *Nat. Nanotechnol.* **4** (2009) 255.
[42] M.P. Schwartz, A.M. Derfus, S.D. Alvarez, S.N. Bhatia and M.J. Sailor // *Langmuir* **22** (2006) 7084.
[43] G.A. Rodriguez, S. Hu and S.M. Weiss // *Opt. Express* **23** (2015) 7111.
[44] L. De Stefano, P. Arcari, A. Lamberti, C. Sanges, L. Rotiroti, I. Rea and I. Rendina // *Sensors* **7** (2007) 214.
[45] G. Rong, A. Najmaie, J.E. Sipe and S.M. Weiss // *Biosens. Bioelectron*. **23** (2008) 1572.
[46] I. Rea, A. Lamberti, I. Rendina, G. Coppola, M. Gioffrè, M. Iodice, M. Casalino, E. De

Tommasi and L. De Stefano // *J. Appl. Phys.* **107** (2010) 014513.
[47] L.M. Bonanno and L.A. DeLouise // *Biosens. Bioelectron.* **23** (2007) 444.
[48] J. Li and M.J. Sailor // *Biosens. Bioelectron.* **55** (2014) 372.
[49] E.J. Szili, A. Jane, S.P. Low, M. Sweetman, P. Macardle, S. Kumar, R.S.C. Smart and N.H. Voelcker // *Sens. Actuators B: Chem*. **160** (2011) 341.
[50] L.M. Bonanno and L.A. DeLouise // *Langmuir* **23** (2007) 5817.
[51] L.A. DeLouise, P.M. Kou and B.L. Miller // *Anal. Chem.* **77** (2005) 1950.
[52] G. Shtenberg, N. Massad-Ivanir, S. Engin, M. Sharon, L. Fruk and E. Segal // *Nanoscale Res. Lett.* **7** (2012) 1.
[53] K. Urmann, S. Arshavsky-Graham, J.G. Walter, T. Scheper and E. Segal // *Analyst* **141** (2016) 5432.
[54] V. Starodub, L. Fedorenko and N. Starodub // *Sens. Actuators B: Chem.* **68** (2000) 40.
[55] S. Li, J. Huang and L. Cai // *Nanotechnology* **22** (2011) 425502.
[56] A.M. Rossi, L. Wang, V. Reipa and T.E. Murphy // *Biosens. Bioelectron*. **23** (2007) 741.
[57] G.A. Rodriguez, J.D. Lonai, R.L. Mernaugh and S.M. Weiss // *Nanoscale Res. Lett*. **9** (2014) 383.
[58] P.S. Chaudhari, A. Gokarna, M. Kulkarni, M.S. Karve and S.V. Bhoraskar // *Sens. Actuators B: Chem.* **107** (2005) 258.
[59] S. Mariani, L.M. Strambini and G. Barillaro // *Anal. Chem*. **88** (2016) 8502.
[60] J. Shang, F. Cheng, M. Dubey, J.M. Kaplan, M. Rawal, X. Jiang, D.S. Newburg, P.A. Sullivan, R.B. Andrade and D.M. Ratner // *Langmuir* **28** (2012) 3338.
[61] L.M. Bonanno, T.C. Kwong and L.A. DeLouise // *Anal. Chem*. **82** (2010) 9711.
[62] L.M. Bonanno and L.A. DeLouise // *Anal. Chem*. **82** (2010) 714.
[63] R. Archer // *J. Phys. Chem. Solids* **14** (1960) 104.
[64] M.T. Kelly, J.K.M. Chun and A.B. Bocarsly // *Appl. Phys. Lett.* **64** (1994) 1693.
[65] R.F. Balderas-Valadez, V. Agarwal and C. Pacholski // *RSC Adv*. **6** (2016) 21430.
[66] Z. Huang, N. Geyer, P. Werner, J. De Boor and U. Gösele // *Adv. Mater.* **23** (2011) 285.
[67] N. Noguchi and I. Suemune // *J. Appl. Phys.* **75** (1994) 476.
[68] O. Andersen, T. Frello and E. Veje // *J. Appl. Phys*. **78** (1995) 6189.
[69] S. Boughaba and K. Wang // *Thin Solid Films* **497** (2006) 83.
[70] M. Saadoun, N. Mliki, H. Kaabi, K. Daoudi, B. Bessaýs, H. Ezzaouia and R. Bennaceur // *Thin Solid Films* **405** (2002) 29.
[71] R.E. Hummel and S.-S. Chang // *Appl. Phys. Lett.* **61** (1992) 1965.
[72] N.H. Maniya, S.R. Patel and Z.V.P. Murthy // *Superlattice. Microst.* **55** (2013) 144.
[73] N.H. Maniya, S.R. Patel and Z.V.P. Murthy // *Rev. Adv. Mater. Sci*. **44** (2016) 257.
[74] V. Lehmann and U. Gosele // *Appl. Phys. Lett*. **58** (1991) 856.
[75] V. Lehmann and U. Gosele // *Adv. Mater*. **4** (1992) 114.
[76] C. Lévy Clément, A. Lagoubi and M. Tomkiewicz // *J. Electrochem. Soc*. **141** (1994) 958.
[77] O. Bisi, S. Ossicini and L. Pavesi // *Surf. Sci. Rep*. **38** (2000) 1.
[78] H. Koyama, N. Shima and N. Koshida // *Phys. Rev. B* **53** (1996) R13291.
[79] M. Thönissen, M.G. Berger, R. Arens-Fischer, O. Glück, M. Krüger and H. Lüth // *Thin Solid Films* **276** (1996) 21.
[80] J. Jakubowicz // *Superlattice. Microst.* **41** (2007) 205.
[81] S.H.C. Anderson, H. Elliott, D.J. Wallis, L.T. Canham and J.J. Powell // *Phys. Status Solidi A* **197** (2003) 331.
[82] M.J. Sailor, *Porous silicon in practice: preparation, characterization and applications* (John Wiley & Sons, 2012).
[83] H.-J. Kim, Y.-Y. Kim, K.-W. Lee, H. Cheng and H. Dong Han // *Physica B* **406** (2011) 1536.
[84] G. Palestino, R. Legros, V. Agarwal, E. Pérez and C. Gergely // *Sens. Actuators B: Chem*. **135** (2008) 27.
[85] L. Pavesi // *La Riv. Del Nuovo Cimento* **20** (1997) 1.
[86] N. Ishikura, M. Fujii, K. Nishida, S. Hayashi and J. Diener // *Infrared Physics & Technology* **53** (2010) 292.
[87] M.G. Berger, R. Arens-Fischer, M. Thönissen, M. Krüger, S. Billat, H. Lüth, S. Hilbrich, W. Theiss and P. Grosse // *Thin Solid Films* **29**7 (1997) 237.
[88] M.J. Sailor and J.R. Link // *Chem. Commun.* (2005) 1375.

[89] T.A. Schmedake, F. Cunin, J.R. Link and M.J. Sailor // *Adv. Mater.* **14** (2002) 1270.
[90] B. Gupta, K. Mai, S.B. Lowe, D. Wakefield, N. Di Girolamo, K. Gaus, P.J. Reece and J.J. Gooding // *Anal. Chem.* **87** (2015) 9946.
[91] B. Guan, A. Magenau, S. Ciampi, K. Gaus, P.J. Reece and J.J. Gooding // *Bioconj. Chem.* **25** (2014) 1282.
[92] S.M. Weiss and X. Wei, In *Handbook of Porous Silicon*, ed. by L.T. Canham (Springer, 2014), p. 815.
[93] Y. Jiao and S.M. Weiss // *Biosens. Bioelectron.* **25** (2010) 1535.
[94] G.A. Rodriguez, J.D. Ryckman, Y. Jiao and S.M. Weiss // *Biosens. Bioelectron.* **53** (2014) 486.
[95] J.L. Heinrich, C.L. Curtis, G.M. Credo, M.J. Sailor and K.L. Kavanagh // *Science* **255** (1992) 66.
[96] N.H. Maniya, S.R. Pate and Z.V.P. Murthy // *Mater. Res. Bull.* **57** (2014) 6.
[97] L.M. Bimbo, M. Sarparanta, H.A. Santos, A.J. Airaksinen, E. Makila, T. Laaksonen, L. Peltonen, V.-P. Lehto, J. Hirvonen and J. Salonen // *ACS nano* **4** (2010) 3023.
[98] Z. Qin, J. Joo, L. Gu and M.J. Sailor // *Part. Part. Syst. Charact.* **31** (2014) 252.
[99] S.O. Meade, M.S. Yoon, K.H. Ahn, M.J. Sailor // *Adv. Mater.* **16** (2004) 1811.
[100] Y.Y. Li, V.S. Kollengode and M.J. Sailor // *Adv. Mater.* **17** (2005) 1249.
[101] S.C. Bayliss, L.D. Buckberry, P.J. Harris and M. Tobin // *J. Porous Mater*. **7** (2000) 191.
[102] S.C. Bayliss, R. Heald, D.I. Fletcher and L.D. Buckberry // *Adv. Mater*. **11** (1999) 318.
[103] L.M. Karlsson, M. Schubert, N. Ashkenov and H. Arwin // *Thin Solid Films* **455-456** (2004) 726.
[104] T. Jay, L.T. Canham, K. Heald, C.L. Reeves and R. Downing // *Phys. Status Solidi A* **182** (2000) 555.
[105] L. Cheng, E. Anglin, F. Cunin, D. Kim, M.J. Sailor, I. Falkenstein, A. Tammewar and W.R. Freeman // *Br. J. Ophthalmol.* **92** (2008) 705.
[106] S.P. Low, N.H. Voelcker, L.T. Canham and K.A. Williams // *Biomaterials* **30** (2009) 2873.
[107] F. Johansson, M. Kanje, C.E. Linsmeier and L. Wallman // I*EEE Trans. Biomed. Eng*. **55** (2008) 1447.
[108] S.D. Alvarez, A.M. Derfus, M.P. Schwartz, S.N. Bhatia and M.J. Sailor // *Biomaterials* **30** (2009) 26.
[109] H.A. Santos, J. Riikonen, J. Salonen, E. Makila, T. Heikkila, T. Laaksonen, L. Peltonen, V.P. Lehto and J. Hirvonen // *Acta Biomater.* **6** (2010) 2721.
[110] E. Korhonen, S. Rönkkö, S. Hillebrand, J. Riikonen, W. Xu, K. Järvinen, V.-P. Lehto and. Kauppinen // *Eur. J. Pharm. Biopharm.* **100** (2016) 1.
[111] A. Nieto, H. Hou, M.J. Sailor, W.R. Freeman and L. Cheng // *Exp. Eye Res.* **116** (2013) 161.
[112] M.A. Shahbazi, M. Hamidi, E.M. Makila, H. Zhang, P.V. Almeida, M. Kaasalainen, J.J. Salonen, J.T. Hirvonen and H.A. Santos // *Biomaterials* **34** (2013) 7776.
[113] J. Salonen, V.-P. Lehto and E. Laine // *Appl. Surf. Sci.* **120** (1997) 191.
[114] J.H. Song and M.J. Sailor // *Inorg. Chem.* **37** (1998) 3355.
[115] G. Mattei, E.V. Alieva, J.E. Petrov and V.A. Yakovlev // *Phys. Status Solidi A* **182** (2000) 139.
[116] K.L. Jarvis, T.J. Barnes and C.A. Prestidge // *Adv. Colloid Interface Sci.* **175** (2012) 25.
[117] R. Boukherroub, S. Morin, D. Wayner and D. Lockwood // *Phys. Status Solidi A* **182** (2000) 117.
[118] R. Boukherroub, J.T.C. Wojtyk, D.D.M. Wayner and D.J. Lockwood // *J. Electrochem. Soc.* **149** (2002) H59.
[119] R. Boukherroub, A. Petit, A. Loupy, J.-N. Chazalviel and F. Ozanam // *J. Phys. Chem. B* **107** (2003) 13459.
[120] M.P. Stewart and J.M. Buriak // *Angew. Chem. Int. Ed.* **37 (**1998) 3257.
[121] M.P. Stewart and J.M. Buriak // *J. Am. Chem. Soc*. **123** (2001) 7821.
[122] J.M. Buriak and M.J. Allen // *J. Am. Chem. Soc.* **120** (1998) 1339.
[123] E.C. Wu, J.S. Andrew, A. Buyanin, J.M. Kinsella and M.J. Sailor // *Chem. Commun*. **47** (2011) 5699.
[124] E.C. Wu, J.S. Andrew, L. Cheng, W.R. Freeman, L. Pearson and M.J. Sailor // *Biomaterials* **32** (2011) 1957.
[125] J. Chapron, S.A. Alekseev, V. Lysenko, V.N. Zaitsev and D. Barbier // *Sens. Actuators B: Chem.* **120** (2007) 706.
[126] K.A. Kilian, T. Bocking and J.J. Gooding // *Chem. Commun.* (2009) 630.

[127] S.N. Jenie, B. Prieto-Simon and N.H. Voelcker // *Biosens. Bioelectron*. **74** (2015) 637.
[128] M. Warntjes, C. Vieillard, F. Ozanam and J.N. Chazalviel // *J. Electrochem. Soc.* **142** (1995) 4138.
[129] V.M. Dubin, C. Vieillard, F. Ozanam and J.N. Chazalviel // *Phys. Status Solidi B* **190** (1995) 47.
[130] F. Erogbogbo, K.-T. Yong, I. Roy, G. Xu, P.N. Prasad and M.T. Swihart // *ACS nano* **2** (2008) 873.
[131] N.Y. Kim and P.E. Laibinis // *J. Am. Chem. Soc.* **120** (1998) 4516.
[132] M.R. Linford, P. Fenter, P.M. Eisenberger and C.E.D. Chidsey // *J. Am. Chem. Soc*. **117** (1995) 3145.
[133] J. Terry, M.R. Linford, C. Wigren, R. Cao, P. Pianetta and C.E. Chidsey // *Appl. Phys. Lett*. **71 (**1997) 1056.
[134] J.H. Song and M.J. Sailor // *J. Am. Chem. Soc*. **120** (1998) 2376.
[135] T. Dubois, F. Ozanam and J. Chazalviel // *Proc. Electrochem. Soc*. **97** (1997) 296.
[136] C.H. De Villeneuve, J. Pinson, M. Bernard and P. Allongue // *J. Phys. Chem. B* **101** (1997) 2415.
[137] C. Gurtner, A.W. Wun and M.J. Sailor // *Angew. Chem. Int. Ed.* 3**8** (1999) 1966.
[138] I.N. Lees, H. Lin, C.A. Canaria, C. Gurtner, M.J. Sailor and G.M. Miskelly // *Langmuir* **19** (2003) 9812.
[139] J. Salonen, V.P. Lehto, M. Björkqvist, E. Laine and L. Niinistö // *Phys. Status Solidi A* **182** (2000) 123.
[140] J. Salonen, E. Laine and L. Niinisto // *J. Appl. Phys*. **91** (2002) 456.
[141] M. Björkqvist, J. Salonen, E. Laine and L. Niinistö // *Phys. Status Solidi A* **197** (2003) 374.
[142] M. Björkqvist, J. Salonen, J. Paski and E. Laine // *Sens. Actuators A: Phys*. **112** (2004) 244.
[143] J. Salonen, M. Björkqvist, E. Laine and L. Niinistö // *Appl. Surf. Sci.* **225** (2004) 389.
[144] M.P. Schwartz, F. Cunin, R.W. Cheung and M.J. Sailor // *Phys. Status Solidi A* **202** (2005) 1380.
[145] A.J. Nijdam, M. Ming-Cheng Cheng, D.H. Geho, R. Fedele, P. Herrmann, K. Killian, V. Espina, E.F. Petricoin, L.A. Liotta and M. Ferrari // *Biomaterials* **28** (2007) 550.
[146] A.S. Anderson, A.M. Dattelbaum, G.A. Montaño, D.N. Price, J.G. Schmidt, J.S. Martinez, W.K. Grace, K.M. Grace and B.I. Swanson // *Langmuir* **24** (2008) 2240.
[147] A. Janshoff, K.-P.S. Dancil, C. Steinem, D.P. Greiner, V.S.-Y. Lin, C. Gurtner, K. Motesharei, M.J. Sailor and M.R. Ghadiri // *J. Am. Chem. Soc*. **120** (1998) 12108.
[148] K.A. Kilian, T. Bocking, K. Gaus, M. Gal and J.J. Gooding // *Biomaterials* **28** (2007) 3055.
[149] R. Vilensky, M. Bercovici and E. Segal // *Adv. Funct. Mater.* **25** (2015) 6725.
[150] F.S.H. Krismastuti, A. Cavallaro, B. Prieto Simon and N.H. Voelcker // *Adv. Sci.* **3** (2016) 1500383.
[151] F.S.H. Krismastuti, S. Pace and N.H. Voelcker // *Adv. Funct. Mater.* **24** (2014) 3639.
[152] H. Qiao, B. Guan, J.J. Gooding and P.J. Reece // *Opt. Express* **18** (2010) 15174.
[153] M. Terracciano, L. De Stefano, N. Borbone, J. Politi, G. Oliviero, F. Nici, M. Casalino, G. Piccialli, P. Dardano, M. Varra and I. Rea // *RSC Adv.* **6** (2016) 86762.
[154] C. Pacholski, C. Yu, G.M. Miskelly, D. Godin and M.J. Sailor // *J. Am. Chem. Soc*. **128** (2006) 4250.
[155] Y. Tang, Z. Li, Q. Luo, J. Liu and J. Wu // *Biosens. Bioelectron.* **79** (2016) 715.
[156] Y. Zhao, G. Gaur, S.T. Retterer, P.E. Laibinis and S.M. Weiss // *Anal. Chem.* **88** (2016) 10940.
[157] O. Syshchyk, V.A. Skryshevsky, O.O. Soldatkin and A.P. Soldatkin // *Biosens. Bioelectron*. **66** (2015) 89.
[158] C. Pacholski, L.A. Perelman, M.S. VanNieuwenhze and M.J. Sailor // *Phys. Status Solidi A* **206** (2009) 1318.
[159] Y. Shang, W. Zhao, E. Xu, C. Tong and J. Wu // *Biosens. Bioelectron.* **25** (2010) 1056.
[160] S.G. Kim, S. Kim, Y.C. Ko, S. Cho and H. Sohn // *Colloids Surf. A* **313-314** (2008) 398.
[161] B. Guan, A. Magenau, K.A. Kilian, S. Ciampi, K. Gaus, P.J. Reece and J.J. Gooding // *Faraday Discuss.* **149** (2011) 301.